Destabilization of mRNAs enhances competence to initiate meiosis in mouse spermatogenic cells

Natalie G. Pfaltzgraff[a], Bingrun Liu[b],
Dirk G. de Rooij[b], David C. Page[b,c,d], and Maria M. Mikedis[a,b,e,1]

[a] Reproductive Sciences Center, Division of Developmental Biology, Cincinnati Children's Hospital Medical Center, Cincinnati, OH, United States
[b] Whitehead Institute, Cambridge, MA, United States
[c] Howard Hughes Medical Institute, Whitehead Institute, Cambridge, MA, United States
[d] Department of Biology, Massachusetts Institute of Technology, Cambridge, MA, United States
[e] Department of Pediatrics, University of Cincinnati College of Medicine, Cincinnati, OH, United States
[1] Correspondence should be addressed to M.M.M. (maria.mikedis@cchmc.org)

Running title: MEIOC enhances competence for meiotic entry

Keywords: MEIOC; RBM46; YTHDC2; germ cells; spermatogenesis

1 **SUMMARY STATEMENT**

2

3 RNA-binding complex MEIOC-YTHDC2-RBM46 destabilizes its mRNA targets, including
4 transcriptional repressors. This activity facilitates the retinoic acid-dependent activation of
5 *Meiosin* gene expression and transition into meiosis.

6

ABSTRACT

The specialized cell cycle of meiosis transforms diploid germ cells into haploid gametes. In mammals, diploid spermatogenic cells acquire the competence to initiate meiosis in response to retinoic acid. Previous mouse studies revealed that MEIOC interacts with RNA-binding proteins YTHDC2 and RBM46 to repress mitotic genes and promote robust meiotic gene expression in spermatogenic cells that have initiated meiosis. Here, we used the enhanced resolution of scRNA-seq, and bulk RNA-seq of developmentally synchronized spermatogenesis, to define how MEIOC molecularly supports early meiosis in spermatogenic cells. We demonstrate that MEIOC mediates transcriptomic changes before meiotic initiation, earlier than previously appreciated. MEIOC, acting with YTHDC2 and RBM46, destabilizes its mRNA targets, including transcriptional repressors *E2f6* and *Mga*, in mitotic spermatogonia. MEIOC thereby derepresses E2F6- and MGA-repressed genes, including *Meiosin* and other meiosis-associated genes. This confers on spermatogenic cells the molecular competence to, in response to retinoic acid, fully activate transcriptional regulator STRA8-MEIOSIN, required for the meiotic G1/S phase transition and meiotic gene expression. We conclude that in mice, mRNA decay mediated by MEIOC-YTHDC2-RBM46 enhances the competence of spermatogenic cells to initiate meiosis.

24 **INTRODUCTION**

25 Sexual reproduction depends on meiosis, a specialized cell cycle that produces haploid gametes
26 via one round of DNA replication followed by two rounds of chromosome segregation. The
27 major chromosomal events of meiosis, including pairing, synapsis, and crossing over of
28 homologous chromosomes, are generally conserved across eukaryotes. By contrast, the
29 mechanisms that govern the transition from mitosis to meiosis are less well conserved (Kimble,
30 2011). For example, in budding yeast, meiotic initiation occurs when multiple inputs converge to
31 activate a master transcription factor (IME1) that upregulates meiotic gene expression (Kassir et
32 al., 1988; Smith et al., 1990; reviewed in van Werven and Amon, 2011). In *Drosophila*
33 *melanogaster*, the transition from mitosis to meiosis occurs via translational repression mediated
34 by the RNA helicase Bgcn and its binding partners Bam and Tut (Chen et al., 2014; Chen et al.,
35 2014; Gonczy et al., 1997; Insco et al., 2009; Insco et al., 2012; McKearin and Spradling, 1990).

36 In mammals, transcriptional activation induced by extrinsic signaling plays a central role
37 in meiotic initiation (i.e., the meiotic G1/S transition). During the transition from mitosis to
38 meiosis (i.e., the "premeiotic" stage during oogenesis and "preleptotene" stage during
39 spermatogenesis), retinoic acid induces meiotic entry by transcriptionally activating *Stra8* and
40 *Meiosin* (Anderson et al., 2008; Baltus et al., 2006; Dokshin et al., 2013; Ishiguro et al., 2020a).
41 *In vitro*, nutrient restriction synergizes with retinoic acid to induce meiotic entry in
42 spermatogenic cells (Zhang et al., 2021). The STRA8-MEIOSIN heterodimer transcriptionally
43 activates expression of G1/S cyclins and meiotic factors that orchestrate the chromosomal events
44 of meiotic prophase I (Anderson et al., 2008; Baltus et al., 2006; Ishiguro et al., 2020a; Kojima et
45 al., 2019; Mark et al., 2008; Soh et al., 2015; Zhang et al., 2023). In mice lacking *Stra8* or
46 *Meiosin* on a C57BL/6 genetic background, premeiotic oogonia and preleptotene spermatocytes
47 halt their development and fail to progress to meiotic prophase I (Anderson et al., 2008; Baltus et
48 al., 2006; Dokshin et al., 2013; Ishiguro et al., 2020a). Indeed, *Stra8*-null premeiotic oogonia and
49 preleptotene spermatocytes, as well as *Meiosin*-null premeiotic oogonia, fail to undergo meiotic
50 DNA replication (Anderson et al., 2008; Baltus et al., 2006; Dokshin et al., 2013; Ishiguro et al.,
51 2020a). (*Meiosin*-null preleptotene spermatocytes initiate an S phase, but it remains unclear
52 whether it is mitotic or meiotic in nature (Ishiguro et al., 2020a).)

53 In the mammalian testis, competence to initiate meiosis in response to retinoic acid is
54 acquired during spermatogenesis. In mitotic spermatogonia, DMRT1 postpones the acquisition

55 of competence, thereby preventing precocious meiotic entry, by repressing retinoic acid-
56 dependent transcription as well as *Stra8* and likely *Meiosin* gene expression (Matson et al. 2010;
57 Ishiguro et al. 2020). As a result, undifferentiated spermatogonia exposed to endogenous retinoic
58 acid express *Stra8* at low levels, and do not express *Meiosin*, and consequently become mitotic
59 differentiating spermatogonia (Ishiguro et al., 2020a; Matson et al., 2010). Differentiating
60 spermatogonia prematurely exposed to exogenous retinoic acid may express STRA8 protein, but
61 they do not initiate meiosis (Endo et al., 2015; Johnson et al., 2023). At the mitosis-to-meiosis
62 transition, the SCF E3 ubiquitin ligase complex degrades DMRT1 (Matson et al., 2010;
63 Nakagawa et al., 2017), thereby conferring upon spermatogenic cells the competence to express
64 *Stra8* and *Meiosin* and initiate meiosis in response to retinoic acid. To date, the SCF complex is
65 the only known positive regulator of spermatogenic cells' competence to initiate meiosis.
66 Post-transcriptional regulation of mRNA also plays a role in governing the mitosis-to-
67 meiosis transition in mammals. After meiotic initiation, MEIOC acts together with RNA helicase
68 YTHDC2 and RNA-binding protein RBM46 to regulate progression through meiotic S phase
69 into meiotic prophase I (Abby et al., 2016; Bailey et al., 2017; Hsu et al., 2017; Jain et al., 2018;
70 Qian et al., 2022; Soh et al., 2017; Wojtas et al., 2017). MEIOC is required to increase meiotic
71 gene expression and also to repress the mitotic cell cycle program, thereby inhibiting a premature
72 and aberrant metaphase several days before wild-type meiotic metaphase I. Consistent with
73 MEIOC, YTHDC2, and RBM46's homology to *Drosophila* proteins Bam, Bgcn, and Tut,
74 respectively, the MEIOC-YTHDC2-RBM46 complex binds to mRNA (Abby et al., 2016; Bailey
75 et al., 2017; Hsu et al., 2017; Jain et al., 2018; Li et al., 2022; Peart et al., 2022; Qian et al., 2022;
76 Saito et al., 2022; Soh et al., 2017). YTHDC2 interacts with exoribonuclease XRN1, while
77 RBM46 recruits nonsense mediated decay protein UPF1 and subunits of the cytoplasmic
78 deadenylase CCR4-NOT complex, which suggests that YTHDC2 and RBM46's mRNA targets
79 are degraded (Kretschmer et al., 2018; Li et al., 2022; Qian et al., 2022; Wojtas et al., 2017). The
80 mechanism by which the MEIOC-YTHDC2-RBM46 complex post-transcriptionally regulates its
81 mRNA targets after meiotic initiation remains poorly defined.
82 Here we molecularly dissect MEIOC's activity in mouse spermatogenic cells during the
83 mitosis-to-meiosis transition via two parallel approaches: (i) single-cell RNA sequencing
84 (scRNA-seq) analysis of postnatal testes and (ii) bulk RNA-seq analysis of developmentally
85 synchronized testes with histologically verified staging. Both approaches reveal that *Meioc*-null

86 germ cells developmentally diverge from wild-type spermatogenic cells at the meiotic G1/S
87 transition, earlier than previously appreciated. Furthermore, we find that MEIOC's activity leads
88 to an increase in meiosis-associated gene expression in late mitotic spermatogonia, before
89 meiotic initiation. We discover that MEIOC destabilizes mRNAs encoding transcriptional
90 repressors of meiotic gene expression. This inhibition of repressors facilitates activation of the
91 master meiotic transcriptional regulator STRA8-MEIOSIN in response to retinoic acid.
92 Therefore, a post-transcriptional repressor of mRNA, acting in parallel to the SCF complex's
93 degradation of DMRT1, enhances spermatogenic cells' competence to activate the meiotic
94 transcriptional regulator and initiate meiosis.

95 **RESULTS**

96 **MEIOC drives a transcriptomic shift at the meiotic G1/S transition**

97 To characterize the molecular consequences of MEIOC activity during spermatogenesis, we
98 performed 10x Genomics Chromium-based scRNA-seq on *Meioc*-null and wild-type P15 testes
99 and identified germ cell clusters by cell type-enriched marker expression and transcriptome-
100 based cell cycle analysis (Fig. S1-3). These germ cell clusters, identified in both wild-type and
101 *Meioc*-null testes, consisted of four clusters in mitosis (undifferentiated spermatogonia [Undiff],
102 differentiating types A_1-A_4 spermatogonia [A1-4], differentiating Intermediate and type B
103 spermatogonia [In/B], and differentiating type B spermatogonia in G2/M phase [B G2M]); three
104 clusters spanning the mitosis-to-meiosis transition (preleptotene spermatocytes in G1, early S,
105 and late S phase [pL G1, pL eS, and pL lS, respectively]); and three clusters in meiotic prophase
106 I (leptotene spermatocytes [L], zygotene spermatocytes [Z], and pachytene spermatocytes [P]).
107 While prior histological characterization found that *Meioc*-null spermatogenic cells to not
108 progress beyond early zygotene (Abby et al., 2016; Soh et al., 2017), some *Meioc*-null cells were
109 designated as pachytene spermatocytes in the scRNA-seq clustering. This indicates
110 transcriptomic progression in *Meioc*-null spermatocytes is not reflected at the histological level.
111 We also identified a cluster composed of *Meioc*-null spermatocytes, which we designated as
112 "Mutant-only" (Mut). As this cluster was primarily comprised of cells in G2/M phase (Fig. S1C),
113 it likely includes the aberrant metaphase spermatogenic cells found in P15 *Meioc*-null testes,
114 days before meiotic metaphase I occurs in the wild-type testis (Abby et al., 2016; Soh et al.,
115 2017).

116 We then applied pseudotime analysis to computationally reconstruct the spermatogenic
117 cells' developmental trajectory from undifferentiated spermatogonia to pachytene spermatocytes
118 (Fig. 1A). *Meioc*-null germ cells followed the same trajectory as wild-type cells during the
119 mitotic stages of spermatogenesis but diverged in the G1 phase of the preleptotene stage, just
120 before meiotic S phase begins. As spermatogenic cells are classically staged via histology, we
121 used histologically-staged samples to independently verify these pseudotime results. We
122 developmentally synchronized spermatogenesis to obtain *Meioc*-null and wild-type testes
123 enriched for preleptotene spermatocytes (Fig. S4A). After histologically verifying staging (Fig.
124 S4B), preleptotene-enriched testes were analyzed via bulk RNA-seq for differential expression,
125 and we identified over 2,000 transcripts as differentially abundant (Fig. S4C). We then asked

126 whether MEIOC impacts the G1/S transition in the preleptotene-enriched testes. We compared
127 percentile ranks for fold changes (WT/*Meioc* KO) for genes enriched at specific cell cycle phases
128 (see Materials and Methods). As a positive control for the disrupted G1/S transition, we re-
129 analyzed a bulk RNA-seq dataset of preleptotene spermatocytes sorted from wild-type and *Stra8*-
130 null testes on a C57BL/6 background (Kojima et al., 2019). This analysis revealed that in
131 preleptotene spermatocytes, MEIOC increased transcript abundance for genes associated with
132 G1/S, S, and G2, similar to STRA8 (Fig. S4D). In total, both scRNA-seq and bulk RNA-seq
133 datasets demonstrate that MEIOC drives a major transcriptomic shift in spermatogenic cells at
134 the meiotic G1/S transition. This is earlier than previously appreciated, as prior histological
135 studies reported that *Meioc*-null spermatogenic cells diverge from wild-type controls after
136 entering meiotic S phase (Abby et al., 2016; Soh et al., 2017).
137

138 **MEIOC begins to affect the abundance of meiotic, rather than mitotic, transcripts before**
139 **the meiotic G1/S transition**

140 MEIOC protein and its binding partner YTHDC2 are first detected immunohistochemically at
141 the preleptotene stage, but YTHDC2 protein is also detected via western blotting in mitotic
142 spermatogonia (Abby et al., 2016; Bailey et al., 2017; Hsu et al., 2017; Jain et al., 2018; Soh et
143 al., 2017; Wojtas et al., 2017). Binding partner RBM46 is detected via immunostaining in mitotic
144 spermatogonia through meiotic spermatocytes (Peart et al., 2022; Qian et al., 2022). We found
145 that *Meioc* and *Ythdc2* transcripts became abundant in late mitotic spermatogonia (In/B and B
146 G2M clusters), while *Rbm46* was highly abundant in all germ cell clusters examined (Fig. 1B).
147 These observations raised the possibility that MEIOC, potentially in collaboration with YTHDC2
148 and RBM46, shapes the germline transcriptome in late mitotic spermatogonia, before the protein
149 can be reliably detected via immunostaining.

150 To assess how MEIOC impacts the transcriptome during spermatogenesis, we carried out
151 scRNA-seq-based differential expression analysis in germ cell clusters associated with mitotic
152 spermatogonia (Undiff, A1-4, In/B, and B G2M clusters), the mitosis-to-meiosis transition (pL
153 G1, eS, and lS clusters), and meiotic prophase I (L and Z clusters), and identified genes whose
154 transcript abundance is increased (log2 fold change WT/*Meioc* KO > 0.1 and adjusted $P < 0.05$)
155 or decreased (log2 fold change WT/*Meioc* KO < -0.1 and adjusted $P < 0.05$) (Fig. 1C) by
156 MEIOC. The number of differentially abundant transcripts increased in the In/B and B G2/M

157 clusters, mirroring *Meioc* and *Ythdc2* expression patterns, and continued to increase thereafter.
158 We conclude that MEIOC begins to affect the germline transcriptome before the meiotic G1/S
159 transition.

160 Based on functional analysis, transcripts upregulated by MEIOC in the In/B through pL
161 lS clusters were enriched for Gene Ontology (GO) annotations related to meiosis (Fig. 1D).
162 Several transcripts contributing to this enrichment became more abundant in mitotic
163 spermatogonia and remained more abundant through early meiotic spermatocytes (Fig. 1E).
164 However, in the L and Z clusters, these changes in meiosis-associated transcripts no longer
165 represented an enrichment in meiosis-associated GO annotations (Fig. 1D). Bulk RNA-seq
166 analysis of preleptotene-enriched testes also revealed enrichment of meiosis-associated factors
167 among MEIOC-upregulated transcripts (Fig. S4C, E). Therefore, MEIOC activity leads to
168 increased meiotic transcript abundance in late mitotic spermatogonia, earlier than previously
169 appreciated. Misregulation of these transcripts provides a molecular rationale for *Meioc*-null
170 spermatogenic cells' delayed progression from preleptotene to leptotene to zygotene stages
171 (Abby et al., 2016; Soh et al., 2017).

172 Given that MEIOC lowers mitotic transcript abundance in fetal oogonia (Soh et al.,
173 2017), we asked whether similar transcriptomic changes were induced by MEIOC in mitotic
174 spermatogonia. MEIOC-downregulated transcripts in the pL lS to Z clusters, but not in
175 developmentally earlier clusters, were enriched for the GO annotation "mitotic cell cycle" (Fig.
176 1D,E). This included mitotic G1/S and G2/M cyclin *Ccna2* (Fig. 1E), whose downregulation was
177 first evident in B G2/M and pL G1 clusters, before the broader enrichment of mitotic cell cycle-
178 associated transcripts was detected. Consistent with MEIOC's downregulation of *Ccna2*
179 transcript abundance, *Meioc*-null spermatocytes exhibit prolonged CCNA2 protein expression at
180 leptotene and zygotene stages, when wild-type spermatocytes no longer express this protein
181 (Abby et al., 2016; Soh et al., 2017). Based on a curated list of genes whose expression is linked
182 to specific cell cycle phases (Hsiao et al., 2020), MEIOC-downregulated genes in pL lS to Z
183 clusters were primarily associated with G2 or M phases (Fig. 1F). We conclude that MEIOC's
184 downregulation of mitotic cell cycle transcripts occurs primarily after the meiotic G1/S
185 transition. The loss of this regulation likely contributes to *Meioc*-null spermatogenic cells'
186 delayed progression from preleptotene to leptotene to zygotene stages; and their premature

187 progression into an aberrant metaphase state during meiotic prophase I (Abby et al., 2016; Soh et
188 al., 2017).
189 In sum, MEIOC elevates the abundance of meiosis-associated transcripts beginning in
190 late transit-amplifying spermatogonia through the mitosis-to-meiosis transition and early meiotic
191 prophase I. Then, late in the mitosis-to-meiosis transition into meiotic prophase I, MEIOC
192 broadly lowers mitotic transcript abundance.
193
194 **MEIOC destabilizes transcripts that it targets**
195 In early spermatocytes, MEIOC localizes to the cytoplasm and interacts with RNA-binding
196 proteins YTHDC2 and RBM46, which recruit other proteins that degrade mRNA (Kretschmer et
197 al., 2018; Li et al., 2022; Qian et al., 2022; Wojtas et al., 2017). Therefore, we hypothesized that
198 MEIOC degrades its mRNA targets. We first defined transcripts that associate with MEIOC by
199 reanalyzing previously published MEIOC RIP-seq data from P15 testes (Soh et al., 2017),
200 identifying 1,991 MEIOC-bound mRNA (Table S6). We assessed the molecular impact of
201 MEIOC's interaction with these transcripts via two approaches. First, we examined these targets'
202 representation among transcripts exhibiting statistically significant abundance changes that were
203 MEIOC-dependent (i.e., MEIOC-upregulated or -downregulated). We found that MEIOC targets
204 were enriched among transcripts whose abundance decreased, but not increased, in response to
205 MEIOC, in the B G2/M through Z clusters (Fig. 2A). Second, we examined all MEIOC targets,
206 irrespective of whether they met a statistical cut-off in the differential expression analysis.
207 MEIOC targets exhibited slightly lower fold changes (WT/KO) than nontargets in the A1-4
208 through Z clusters (Fig. 2B). An analysis of estimated changes in transcript stability from bulk
209 RNA-seq data showed that MEIOC targets had reduced transcript stability relative to nontargets
210 (Fig. S6A). Therefore, MEIOC lowers the abundance of transcripts that it targets, presumably by
211 promoting their degradation, beginning in mitotic spermatogonia.
212 Given MEIOC's interaction with YTHDC2 and RBM46, we hypothesized that many
213 MEIOC targets are also bound by YTHDC2 and RBM46. Based on a published YTHDC2 CLIP
214 analysis from testes (Saito et al., 2022) and our reanalysis of RBM46 CLIP data from testes
215 (Qian et al., 2022), MEIOC shared 202 mRNA targets with YTHDC2 and 1,477 targets with
216 RBM46, both of which are statistically significant overlaps (Fig. 2C). The three proteins had 187
217 mRNA targets in common. Only 15 mRNAs were bound by MEIOC and YTHDC2 but not

218 RBM46, and these likely represent technical differences between datasets rather than a
219 biologically meaningful group of transcripts. MEIOC-YTHDC2-RBM46 targets were enriched
220 for GO annotations associated with RNA stability, while MEIOC-RBM46-only targets did not
221 exhibit statistically significant enrichment (Table S6). We conclude that MEIOC shares many,
222 but not all, of its mRNA targets with YTHDC2 and RBM46.

223 As YTHDC2 and RBM46 interact with proteins that degrade mRNA, we hypothesized
224 that MEIOC has a greater impact on transcript stability when acting in partnership with
225 YTHDC2 and RBM46 than when acting alone. To test this, we binned MEIOC's targets as
226 follows: MEIOC-YTHDC2-RBM46 targets, MEIOC-RBM46-only targets, MEIOC-YTHDC2-
227 only, and MEIOC-only targets. We compared how these groups of target genes respond to
228 MEIOC in our scRNA-seq data. First, we examined whether each group was overrepresented
229 among transcripts whose abundance decreased in response to MEIOC. MEIOC-YTHDC2-
230 RBM46 targets exhibited such enrichment beginning in mitotic spermatogonia (Fig. 2D). By
231 contrast, MEIOC-YTHDC2-only targets were enriched in one meiotic cluster and MEIOC-only
232 targets showed no such enrichment (Fig. 2D). MEIOC-RBM46-only targets were enriched
233 beginning at the mitosis-to-meiosis transition (Fig. 2D), suggesting that MEIOC-RBM46 may
234 impact the transcriptome independent of YTHDC2, but the biological significance of this
235 regulation remains unclear. Second, we examined the effect of YTHDC2 and RBM46 on the
236 stability of MEIOC targets, irrespective of statistical cutoff. Relative to MEIOC-only targets,
237 MEIOC-YTHDC2-RBM46 targets exhibited the largest decrease in transcript abundance in all
238 scRNA-seq germ cell clusters (Fig. 2E), as well as in transcript stability in the bulk RNA-seq
239 analysis of preleptotene-enriched testes (Fig. S5B, S6B). Taken together, these data demonstrate
240 that MEIOC's destabilization of its target mRNAs occurs via its interaction with both YTHDC2
241 and RBM46.

242 Given that MEIOC-downregulated transcripts are enriched for mitotic cell cycle factors,
243 we hypothesized that MEIOC-YTHDC2-RBM46 directly targets and destabilizes these factors.
244 By comparing MEIOC-downregulated transcripts bearing the GO annotation "mitotic cell cycle"
245 with MEIOC-YTHDC2-RBM46 targets, we discovered a small but statistically significant
246 overlap that included factors that impact cell cycle progression, such as *Ccna2* and *E2f6* (Fig.
247 2F). Some targets were downregulated by MEIOC in mitotic spermatogonia and early in the
248 mitosis-to-meiosis transition, before mitotic cell cycle enrichment was evident among the

249 MEIOC-downregulated genes (Fig. 1C,D). Therefore, MEIOC's destabilization of mRNAs
250 before and during the mitosis-to-meiosis transition may impact spermatogenic cells' ability to
251 establish a meiosis-specific cell cycle program in meiotic prophase I.
252 We also considered the possibility that some MEIOC-YTHDC2-RBM46 targets are
253 stabilized, rather than destabilized, by the complex. In particular, given that MEIOC-upregulated
254 transcripts are enriched for the "meiotic cell cycle" annotation (Fig. 1C,D), we asked whether
255 these transcripts were MEIOC-YTHDC2-RBM46 targets. MEIOC-upregulated "meiotic cell
256 cycle" transcripts and MEIOC-YTHDC2-RBM46 targets shared one transcript, *Meioc* (Fig. 2F),
257 with this overlap representing neither statistical depletion nor enrichment. We conclude that
258 MEIOC-YTHDC2-RBM46 does not directly regulate the stability of meiosis-associated
259 transcripts.
260 In total, MEIOC collaborates with YTHDC2 and RBM46 to promote the decay of the
261 transcripts that it targets, beginning in mitotic spermatogonia.
262
263 **MEIOC's destabilization of *E2f6* and *Mga* transcripts elevates expression of E2F6- and**
264 **MGA-repressed genes**
265 Most MEIOC-regulated transcripts, as defined by RNA-seq analysis of wild-type versus *Meioc*-
266 null samples, do not directly interact with MEIOC-YTHDC2-RBM46 (Fig. 3A, S6C). We
267 examined whether these changes in transcript abundance reflected altered transcriptional rates or
268 altered transcript stabilities. Applying REMBRANDTS to our bulk RNA-seq data, we estimated
269 changes in mRNA abundance from changes in exonic reads, changes in pre-mRNA abundance
270 (i.e., transcriptional rate) from changes in intronic reads, and changes in mRNA stability from
271 the difference between the changes in exonic and intronic reads (Alkallas et al., 2017; Gaidatzis
272 et al., 2015). MEIOC-regulated transcripts exhibited large changes in transcriptional rates and
273 smaller changes in transcript stabilities (Fig. 3B). We conclude that MEIOC indirectly impacts
274 transcription in ways that alter the abundance of transcripts that it does not bind.
275 We set out to identify MEIOC targets that might drive such transcriptional changes. The
276 vast majority of MEIOC-upregulated transcripts are not directly bound by MEIOC (Fig. 2A, 3A).
277 We hypothesized that MEIOC-YTHDC2-RBM46 destabilizes a mRNA that encodes a
278 transcriptional repressor; destabilization of this mRNA then derepresses (i.e., upregulates) gene
279 expression. For this analysis, we focused on the In/B to pL G1 clusters, before spermatogenic

280 cells have undergone the MEIOC-dependent transcriptomic shift observed in the scRNA-seq
281 pseudotime analysis (Fig. 1A,B). Among 48 MEIOC-YTHDC2-RBM46 targets downregulated
282 by MEIOC in the In/B to pL G1 clusters, we identified eight mRNAs that encode transcriptional
283 repressors: *Cbx1*, *E2f6*, *Hnrnpab*, *Mga*, *Pbrm1*, *Rad21*, *Sp3*, and *Suz12* (Fig. 3C,D). Strikingly,
284 *Cbx1*, *E2f6,* and *Mga* all encode subunits of the noncanonical Polycomb Repressive Complex
285 (PRC) 1.6 (Fig. S7A, S9A), representing a statistically significant enrichment for the complex's
286 subunits (one-tailed hypergeometric test, P = 3.55E-05). *E2f6* and *Mga* are particularly attractive
287 candidates because they encode sequence-specific DNA-binding subunits of PRC1.6 required to
288 repress meiosis-specific genes in somatic and embryonic stem cells (Pohlers et al. 2005; Dahlet
289 et al. 2021; Kehoe et al. 2008; Maeda et al. 2013; Suzuki et al. 2016; Kitamura et al. 2021;
290 Uranishi et al. 2021). By contrast, CBX1 is not strictly required to repress gene expression, as
291 other CBX proteins can compensate for its absence (Ostapcuk et al., 2018).
292 We hypothesized that MEIOC-YTHDC2-RBM46's inhibition of *E2f6* and *Mga* impacts
293 gene expression during spermatogenesis. To test this, we reanalyzed ChIP-seq and RNA-seq
294 datasets from mouse embryonic stem cells (Dahlet et al., 2021; Qin et al., 2021; Stielow et al.,
295 2018) to identify genes directly repressed by E2F6 or MGA (see Materials and Methods; Fig.
296 S8A,B). Given that genetic ablation of *Max* (which encodes MGA's binding partner and a
297 PRC1.6 subunit) induces embryonic stem cells to enter meiosis (Suzuki et al., 2016), these data
298 are relevant to meiotic entry in spermatogenic cells. As E2F6 and MGA cooperate to repress
299 expression of an overlapping set of genes (Dahlet et al., 2021) (Fig. S8C), we classified genes as
300 repressed by both E2F6 and MGA, repressed by E2F6 alone, or repressed by MGA alone. Genes
301 repressed by both E2F6 and MGA, but not those repressed by either factor alone, were
302 overrepresented among MEIOC-upregulated transcripts beginning in the mitotic In/B cluster
303 (Fig. 3E), coinciding with MEIOC's destabilization of *Mga* mRNA in that cluster (Fig. 3D). This
304 overrepresentation continued through the mitosis-to-meiosis transition (Fig. 3E), including the
305 pL G1 cluster when MEIOC destabilizes *E2f6* and *Mga* mRNA (Fig. 3D). Genes repressed by
306 both E2F6 and MGA were not enriched among MEIOC-downregulated transcripts (Fig. 3E).
307 Bulk RNA-seq analysis of preleptotene-enriched testes largely confirmed these results, while
308 also revealing that MEIOC-upregulated genes were enriched for genes repressed by E2F6 or
309 MGA alone (Fig. S9B), likely because this analysis included lowly expressed genes that were not
310 detected in the sparser scRNA-seq dataset. We conclude that MEIOC's repression of E2F6 and

311 MGA results in enhanced expression of specific genes in mitotic spermatogonia.
312 We also examined whether MEIOC's repression of E2F6 and MGA results in diminished
313 expression of other genes in spermatogenic cells. For this analysis, we used the mouse
314 embryonic stem cell datasets to classify genes as activated by both E2F6 and MGA, by E2F6
315 alone, or by MGA alone. Genes activated by MGA alone were modestly enriched among
316 MEIOC-downregulated genes within a limited set of clusters (pL lS and L; Fig. S8D). By
317 contrast, genes activated by both E2F6 and MGA or by E2F6 alone were not enriched among
318 MEIOC-upregulated (or downregulated) genes (Fig. S8D). Bulk RNA-seq analysis of
319 preleptotene-enriched testes confirmed these results (Fig. S9B). We conclude that MEIOC's
320 repression of E2F6 and MGA leads to upregulation of gene expression.
321 As many MEIOC-upregulated transcripts are meiotic cell cycle factors not bound by
322 MEIOC-YTHDC2-RBM46 (Fig. 1D, 2F), we hypothesized that repression of E2F6 and MGA
323 enhances expression of these meiotic genes. To test this, we asked whether E2F6- and MGA-
324 repressed genes are enriched among meiotic cell cycle transcripts upregulated by MEIOC. We
325 again focused this analysis on the In/B to pL G1 clusters, before spermatogenic cells undergo
326 MEIOC-dependent transcriptomic changes. We found that 13 of 17 MEIOC-upregulated meiotic
327 cell cycle transcripts are targeted for repression by E2F6 and/or MGA (Fig. 3F), and we
328 confirmed these observations in bulk RNA-seq analysis of preleptotene-enriched testes (Fig.
329 S9C). We conclude that MEIOC's destabilization of *E2f6* and *Mga* mRNAs de-represses
330 meiosis-associated gene expression beginning in mitotic spermatogonia.
331
332 **MEIOC indirectly activates transcriptional regulator STRA8-MEIOSIN to enhance**
333 **spermatogenic cells' competence to initiate meiosis**
334 In mouse embryonic stem cells, E2F6 and MGA directly repress *Meiosin* (*Gm4969*, *Bhmg1*)
335 (Uranishi et al., 2021) (Fig. S8A,B). Consistent with MEIOC's destabilization of *E2f6* and *Mga*
336 mRNAs, we found that MEIOC enhances *Meiosin* expression at both the transcript and protein
337 levels during the mitosis-to-meiosis transition (Fig. 4A, S4C, S10A). By meiotic prophase I,
338 *Meioc*-null germ cells exhibited delayed upregulation of *Meiosin* expression (Fig. 4A). We
339 confirmed that *Meiosin* expression is also increased by YTHDC2 and RBM46, based on our
340 examination of published RNA-seq data from postnatal testes (Jain et al., 2018; Peart et al.,

341 2022). MEIOC protein does not bind *Meiosin* mRNA (Table S6). This suggests that MEIOC-
342 YTHDC2-RBM46's regulation of *E2f6* and *Mga* may be impacting *Meiosin* gene expression.
343 We examined whether MEIOC affects other known regulators of *Meiosin* gene
344 expression. As retinoic acid transcriptionally activates *Meiosin* (Ishiguro et al., 2020b), we
345 considered whether MEIOC enhances retinoic acid-mediated transcription, but we found no
346 evidence for this model. MEIOC did not increase the transcript abundance of any retinoic acid
347 receptor (RAR) or retinoid X receptor (RXR), which mediate transcriptional activation by
348 retinoic acid (reviewed in Endo et al., 2019) (Fig. S10B,C). In addition, MEIOC did not
349 upregulate additional retinoic acid-activated genes *Stra8*, which encodes MEIOSIN's binding
350 partner, and *Rec8*, a meiotic cohesin (Koubova et al., 2014; Soh et al., 2015; Zhang et al., 2021)
351 (Fig. 4A, S10C,D). We observed that MEIOC downregulated *Stra8* abundance overall in the
352 scRNA-seq data (Fig. 4A), but as *Stra8* mRNA is not directly bound by MEIOC (Table S6), the
353 molecular basis for this regulation remains uncharacterized. These observations indicate that
354 MEIOC does not activate *Meiosin* gene expression by increasing retinoic acid-mediated
355 transcription.
356 We also considered whether *Dmrt1*, whose encoded protein presumably represses
357 *Meiosin* gene expression (Ishiguro et al., 2020b), was regulated by MEIOC-YTHDC2-RBM46,
358 but again, we found no evidence for this alternative model. *Dmrt1* transcript was not a target of
359 MEIOC, YTHDC2, or RBM46 (Table S6), nor was it differentially expressed in response to
360 MEIOC in the pL G1 or pL eS clusters of the scRNA-seq analysis or in the preleptotene-enriched
361 testes of the bulk RNA-seq analysis (Fig. S11A,B). DMRT1 protein expression was similar in
362 both wild-type and *Meioc*-null testes, with DMRT1 expressed in mitotic spermatogonia but
363 absent from preleptotene spermatocytes (Fig. S11C). In addition, MEIOC did not affect the
364 expression of DMRT1-regulated genes *Tbx1* and *Crabp2* (Matson et al., 2010) (Fig. S11D,E).
365 DMRT1 also directly inhibits *Stra8* expression (Matson et al., 2010), but as noted above, *Stra8*
366 was not activated by MEIOC (Fig. 4A). Therefore, changes in DMRT1 do not account for
367 MEIOC's upregulation of *Meiosin* gene expression. Taking these observations together, we
368 conclude that MEIOC's repression of *E2f6* and *Mga* derepresses *Meiosin* gene expression during
369 the mitosis-to-meiosis transition.
370 STRA8-MEIOSIN functions as an obligate heterodimer that transcriptionally activates
371 gene expression during the mitosis-to-meiosis transition (Ishiguro et al., 2020a; Kojima et al.,

372 2019). As described above, *Stra8* is highly expressed at both the transcript and protein levels in
373 *Meioc*-null spermatogenic cells at the mitosis-to-meiosis transition (Fig. 4A, S4C, Fig. S10A), as
374 previously reported (Abby et al., 2016; Soh et al., 2017). We hypothesized that MEIOC's
375 upregulation of *Meiosin* gene expression leads to STRA8-MEIOSIN-mediated transcriptional
376 changes. We tested three predictions of this hypothesis.

377 First, we tested whether, during the mitosis-to-meiosis transition, genes dependent on
378 MEIOC also depend on STRA8. We defined STRA8-dependent (i.e., STRA8-upregulated or -
379 downregulated) genes using bulk RNA-seq data from wild-type and *Stra8*-null preleptotene
380 spermatocytes isolated via synchronization and sorting (Kojima et al., 2019). STRA8-
381 upregulated genes were enriched among MEIOC-upregulated genes during the mitosis-to-
382 meiosis transition (pL eS and lS clusters) and in meiotic prophase I (L cluster; Fig. 4B).
383 Similarly, STRA8-downregulated transcripts were enriched among MEIOC-downregulated
384 transcripts at these same stages (Fig. 4B). Bulk RNA-seq analysis of preleptotene-enriched testes
385 produced similar results (Fig. S12A).

386 Second, focusing exclusively on STRA8-dependent genes, we looked for correlated
387 changes in transcript abundance in the MEIOC scRNA-seq and STRA8 bulk RNA-seq datasets.
388 STRA8-dependent genes exhibited significantly correlated effects in the MEIOC and STRA8
389 datasets that peaked at the mitosis-to-meiosis transition (pL eS and lS clusters; Fig. 4C, S13A,
390 S14A). STRA8-dependent genes similarly exhibited robustly correlated effects in the MEIOC
391 bulk RNA-seq dataset from preleptotene-enriched testes and the STRA8 dataset (Fig. S12B). We
392 conclude that MEIOC activity leads to STRA8-MEIOSIN-mediated changes in transcript
393 abundance.

394 Third, we tested whether MEIOC-dependent genes are directly activated by STRA8-
395 MEIOSIN. We identified STRA8-activated genes as those genes (i) whose expression increased
396 in response to STRA8 and (ii) whose promoters were bound by STRA8 (as defined by ChIP-seq
397 from testes enriched for preleptotene spermatocytes (Kojima et al., 2019)). We found that
398 MEIOC-upregulated genes were enriched for STRA8-activated genes during the mitosis-to-
399 meiosis transition (pL eS and lS clusters; Fig. 4D). However, de novo motif analysis failed to
400 identify enrichment of any motif among these MEIOC-upregulated genes, likely due to the
401 sparsity of scRNA-seq data. The enrichment of STRA8-activated genes among MEIOC-
402 upregulated genes was also visible in the bulk RNA-seq analysis of preleptotene-enriched testes

403 (Fig. S12C). Furthermore, the top motif identified by de novo motif analysis of MEIOC-
404 upregulated genes from the bulk RNA-seq analysis matched the STRA8-MEIOSIN binding
405 motif (Fig. S12D). The second top motif matched the binding site shared by E2F6 and other E2F
406 proteins (Fig. 12D), as previously reported among STRA8-activated genes (Kojima et al., 2019).
407 In total, ~60-70% of MEIOC-upregulated genes are directly activated by STRA8-MEIOSIN.
408 Together, these analyses demonstrate that MEIOC indirectly activates the STRA8-
409 MEIOSIN transcriptional regulator, thereby facilitating a massive shift in the transcriptome at
410 the meiotic G1/S transition (Fig. 1A). With this new molecular insight, we revisited our
411 interpretation of the *Meioc*-null phenotype. Based on prior histological analyses and DNA
412 labeling experiments, *Meioc*-null spermatogenic cells successfully enter the preleptotene stage,
413 express STRA8 protein, and exhibit DNA synthesis. However, they then accumulate at the
414 preleptotene stage and are delayed in entering meiotic prophase I (Abby et al., 2016; Soh et al.,
415 2017). Previously, we interpreted these data as *Meioc*-null spermatogenic cells successfully
416 undergoing the meiotic G1/S phase transition but thereafter exhibiting disrupted progression into
417 meiotic prophase I. Given our present findings that *Meioc*-null germ cells are delayed in
418 upregulating *Meiosin* expression and exhibit a disrupted meiotic G1/S phase transition, we now
419 interpret the *Meioc*-null phenotype as defective meiotic initiation. We conclude that MEIOC
420 enhances spermatogenic cells' competence to initiate meiosis by activating the STRA8-
421 MEIOSIN transcriptional regulator.
422
423 **MEIOC derepresses meiotic gene expression before activating STRA8-MEIOSIN**
424 We observed that many STRA8-activated genes are repressed by E2F6 and/or MGA (Fig. S12E).
425 Consistent with this observation, STRA8-activated genes are enriched for the binding motif of
426 E2F6 and other E2F proteins (Fig. 12D; Kojima et al., 2019). Accordingly, we divided STRA8-
427 activated genes into two groups, based on whether or not they were directly repressed by E2F6
428 and/or MGA in embryonic stem cells. As MEIOC represses E2F6 and MGA in mitotic
429 spermatogonia and activates STRA8-MEIOSIN during the mitosis-to-meiosis transition, we
430 predicted that genes experimentally defined as E2F6 and/or MGA-repressed and STRA8-
431 activated would be upregulated by MEIOC starting in mitotic spermatogonia, coincident with
432 MEIOC's destabilization of *E2f6* and *Mga* mRNAs. Conversely, STRA8-activated genes not
433 repressed by E2F6 or MGA should be upregulated by MEIOC later in the mitosis-to-meiosis

434 transition, coincident with MEIOC-mediated upregulation of *Meiosin* gene expression.
435 Consistent with these predictions, STRA8-activated, E2F6-MGA-repressed genes were enriched
436 among MEIOC-upregulated genes in the mitotic B G2/M cluster and during the mitosis-to-
437 meiosis transition (pL G1, eS, and lS clusters; Fig. 4E). Also as predicted, STRA8-activated
438 genes not repressed by E2F6 or MGA exhibited enrichment in the pL eS and lS clusters (Fig.
439 4E). Both gene sets were also enriched among MEIOC-upregulated genes in the bulk RNA-seq
440 analysis (Fig. S12F). We conclude that, during late transit amplification, MEIOC derepresses a
441 set of meiotic genes targeted by E2F6 and MGA; then during the mitosis-to-meiosis transition,
442 MEIOC elevates expression of these and other meiotic genes by activating STRA8-MEIOSIN.
443 In total, MEIOC-YTHDC2-RBM46's destabilization of *E2f6* and *Mga* mRNAs in late
444 mitotic spermatogenic cells derepresses E2F6-MGA-targeted genes, including *Meiosin* and other
445 meiosis-associated genes. In turn, these steps drive activation of the STRA8-MEIOSIN
446 transcriptional regulator by retinoic acid during the mitosis-to-meiosis transition (Fig. 5). As
447 STRA8-MEIOSIN is the molecular vehicle through which retinoic acid induces the meiotic G1/S
448 transition, MEIOC's regulation of the STRA8-MEIOSIN complex enhances spermatogenic cells'
449 competence to initiate meiosis.

450 **DISCUSSION**

451 Here we demonstrate that *Meioc*-null spermatogenic cells developmentally diverge from their
452 wild-type counterparts during the meiotic G1/S transition, earlier than previously appreciated.
453 MEIOC is required to derepress expression of meiotic genes, including the transcriptional
454 regulator *Meiosin*. In turn, MEIOC elevates expression of genes targeted by STRA8-MEIOSIN,
455 which drives meiotic initiation. Therefore, MEIOC enhances spermatogenic cells' competence to
456 activate the meiotic transcriptional regulator and initiate meiosis in response to retinoic acid.

457 We find that MEIOC-YTHDC2-RBM46 destabilizes its mRNA targets, as suggested
458 previously based on analyses of transcript abundance (Hsu et al., 2017; Qian et al., 2022; Saito et
459 al., 2022; Soh et al., 2017). Here we distinguished changes in transcription vs. transcript stability
460 via two approaches. First, scRNA-seq allowed us to identify and analyze spermatogenic cells
461 impacted by MEIOC before the onset of major transcriptional changes. Second, we employed a
462 specialized pipeline to distinguish between transcriptional rate and RNA stability in bulk RNA-
463 seq data of preleptotene-enriched testes (Alkallas et al., 2017). These complementary methods
464 confirmed that MEIOC-YTHDC2-RBM46 reduces the stability of its target transcripts.
465 Transcript stability may be the primary mechanism by which MEIOC-YTHDC2-RBM46
466 regulates its targets, as a recent study using ribosome profiling found that YTHDC2 does not
467 affect translation in postnatal testes (Saito et al., 2022).

468 MEIOC-YTHDC2-RBM46 elevates the abundance of meiosis-associated transcripts
469 without binding them. Here we demonstrated that these transcript abundance changes are driven
470 by changes in transcription (Fig. 3B). Further, we provide a two-step mechanism for these
471 indirect effects on transcript abundance. First, MEIOC-YTHDC2-RBM46 binds to and
472 destabilizes *E2f6* and *Mga* mRNAs, which encode transcriptional repressors whose genomic
473 targets are enriched for meiosis-associated genes (Dahlet et al., 2021; Kehoe et al., 2008;
474 Kitamura et al., 2021; Maeda et al., 2013; Pohlers et al., 2005; Suzuki et al., 2016; Uranishi et
475 al., 2021). This regulation impacts gene expression, and potentially differentiation, beginning in
476 late mitotic spermatogonia, when MEIOC begins to destabilize *Mga* (Fig. 3D). Second, this
477 MEIOC-YTHDC2-RBM46-mediated repression of *E2f6* and *Mga* derepresses *Meiosin* gene
478 expression and activates STRA8-MEIOSIN. This transcriptional regulator then activates meiotic
479 gene expression and the meiotic G1/S transition. Thus, MEIOC-YTHDC2-RBM46's repression
480 of a transcriptional repressor confers developmental competence to initiate meiosis.

481 MEIOC is also required in meiotic oocytes for progression through early meiotic
482 prophase I (Abby et al., 2016; Soh et al., 2017), and it remains an open question whether MEIOC
483 supports activation of STRA8-MEIOSIN during meiotic initiation in premeiotic oogonia. There
484 are some molecular differences in meiotic initiation between oogonia and spermatogenic cells.
485 At stages when wild-type germ cells are undergoing meiotic DNA replication, *Stra8*-null
486 oogonia fail to initiate any DNA replication, while *Stra8*-null spermatogenic cells initiate a DNA
487 replication that is non-meiotic in nature, as meiotic cohesin REC8 is not loaded onto the
488 chromosomes (Anderson et al., 2008; Baltus et al., 2006; Dokshin et al., 2013). STRA8 has the
489 additional function of sequestering RB1, a key regulator of the G1/S transition, to promote a
490 timely meiotic G1/S transition in oogonia, but this activity does not appear to impact
491 spermatogenesis (Shimada et al., 2023).
492 In mitotic oogonia, loss of PRC1 activity via genetic ablation of *Ring1* and *Rnf2* causes
493 premature meiosis due to precocious expression of *Stra8* and other meiosis-associated genes
494 (Yokobayashi et al., 2013). In addition, genetic ablation of *Max,* which encodes a subunit of
495 PRC1.6, induces a similar phenotype with precocious expression of *Stra8*, *Meiosin*, and meiosis-
496 associated genes (Suzuki et al., 2024). During spermatogenesis, PRC1.6 may also regulate gene
497 expression and meiotic initiation, but the germline roles for PRC1.6, E2F6, or MGA remain
498 uncharacterized. While *E2f6*-null mice are fertile, spermatogenesis was reportedly disrupted,
499 without detailed characterization (Storre et al., 2002). Genetic ablation of *Mga* causes embryonic
500 lethality, precluding analysis of spermatogenesis (Burn et al., 2018; Washkowitz et al., 2015).
501 Further studies will be required to characterize E2F6 and MGA's roles in spermatogenesis,
502 including whether loss of E2F6 and MGA rescues the developmental competence of *Meioc*-null
503 spermatogenic cells. Other transcriptional repressors targeted by MEIOC-YTHDC2-RBM46
504 may also control *Meiosin* gene expression.
505 As some *Meioc*-null spermatogenic cells upregulate *Meiosin* gene expression and enter
506 meiotic prophase I on a delayed timeline, MEIOC is not strictly required for competence to
507 initiate meiosis. Perhaps residual activity of YTHDC2-RBM46 in the absence of MEIOC can
508 support meiotic initiation in some cells. Consistent with this possibility, YTHDC2 protein is still
509 expressed in *Meioc*-null spermatogenic cells (Abby et al., 2016; Soh et al., 2017), but whether
510 loss of MEIOC affects RBM46 protein expression remains unclear. Alternatively, acquisition of
511 competence mediated by the SCF complex may enable meiotic initiation on this delayed

512 timeline. Regardless, we have found that the *Meioc*-null, *Ythdc2*-null, or *Rbm46*-null phenotype
513 of delayed entry into meiotic prophase I is the result of reduced STRA8-MEIOSIN
514 transcriptional activation and is less severe than the arrest at the G1/S transition, before meiotic
515 prophase I, exhibited by *Stra8*-null or *Meiosin*-null spermatogenic cells on an inbred C57BL/6
516 background. Intriguingly, *Stra8*-null spermatogenic cells on a mixed genetic background exhibit
517 the less severe phenotype seen with *Meioc*-null, *Ythdc2*-null, or *Rbm46*-null spermatogenic cells.
518 Our analyses of the *Meioc*-null phenotype suggest that, on a mixed genetic background, *Stra8*-
519 null spermatogenic cells transcriptionally activate some meiotic gene expression, perhaps due to
520 MEIOSIN acting as a homodimer, but further studies will be required to test this possibility.
521 Our model of mammalian meiotic initiation exhibits parallels to the molecular network
522 that governs meiotic initiation in budding yeast. In yeast, inhibition of a transcriptional repressor
523 (Rme1p) via mRNA destabilization activates expression of the key transcription factor (Ime1p)
524 that governs meiotic entry. We conclude that in both unicellular eukaryotes and multicellular
525 organisms, destabilization of a transcriptional repressor at the transcript level controls activation
526 of the meiotic transcriptional program.
527 We have placed transcriptional activation by STRA8-MEIOSIN and post-transcriptional
528 repression of mRNA by MEIOC-YTHDC2-RBM46 in a positive feedback loop that facilitates
529 the mitosis-to-meiosis transition (Fig. 5). This model generates a new question: how is MEIOC-
530 YTHDC2-RBM46 activated before retinoic acid activates STRA8-MEIOSIN, particularly when
531 E2F6 and MGA repress *Meioc* gene expression (Fig. 5)? One possibility is illustrated by
532 MEIOC's *Drosophila* homolog Bam, which (translationally) represses its mRNA targets in late
533 mitotic spermatogonia to facilitate the transition from mitosis to meiosis (Insco et al., 2009;
534 Insco et al., 2012). This transition requires that Bam protein accumulates to a critical threshold
535 level (Insco et al., 2009). Whether mammalian MEIOC protein levels must also clear a critical
536 threshold to activate the MEIOC-YTHDC2-RBM46 complex requires further investigation.
537 In conclusion, by destabilizing its mRNA targets, MEIOC-YTHDC2-RBM46 represses
538 transcriptional repressors E2F6 and MGA, thereby allowing spermatogenic cells to activate
539 *Meiosin* expression in response to retinoic acid. In turn, this activates the key meiotic
540 transcriptional regulator STRA8-MEIOSIN, which amplifies expression of meiosis- and cell
541 cycle-associated genes and drives the meiotic G1/S transition. In total, the post-transcriptional
542 activity of MEIOC-YTHDC2-RBM46 enhances the activity of the meiotic transcriptional

543 regulator. This regulatory pathway, acting in parallel with SCF complex-mediated degradation of
544 DMRT1, enhances spermatogenic cells' competence to initiate meiosis in response to retinoic
545 acid.

546 **MATERIALS AND METHODS**

547 *Animals*

548 All experiments involving mice were performed in accordance with the guidelines of the
549 Massachusetts Institute of Technology (MIT) Division of Comparative Medicine and Cincinnati
550 Children's Hospital Medical Center (CCHMC) Division of Veterinary Services, which are
551 overseen by their respective Institutional Animal Care and Use Committees (IACUC). The
552 animal care programs at MIT/Whitehead Institute and CCHMC are accredited by the Association
553 for Assessment and Accreditation of Laboratory Animal Care, International (AAALAC) and
554 meet or exceed the standards of AAALAC as detailed in the Guide for the Care and Use of
555 Laboratory Animals. This research was approved by the MIT IACUC (no. 0617-059-20) and
556 CCHMC IACUC (no. 2022-0061).

557 Mice carrying the *Meioc*-null allele *Meioc*$^{tm1.1Dpc}$ (Soh et al., 2017) were backcrossed to
558 C57BL/6N (B6N) from Taconic Biosciences for at least 10 generations. Mice used for scRNA-
559 seq experiments were also heterozygous for *Hspa2*^{tm1Dix} (RRID: IMSR_JAX:013584;(Dix et al.,
560 1996)) and homozygous for *Gt(ROSA)26Sor*$^{tm9(CAG\text{-}tdTomato)Hze}$ (*ROSA26*^{tdTomato};
561 RRID:IMSR_JAX:007909; (Madisen et al., 2010)) with the floxed stop codon intact; both of
562 these genotypes exhibit normal spermatogenesis.

563

564 *10x Genomics single-cell RNA-seq*

565 Single-cell sequencing libraries were prepared and sequenced in two batches, with each batch
566 containing one wild-type and one *Meioc*-null pup at P15. One P15 testis per pup was
567 enzymatically dissociated into single cells (see Supplementary Material and Methods) and
568 resuspended in 0.05% bovine serum albumin (BSA) in phosphate buffered saline (PBS) for a
569 target concentration of 1000 cells per microliter. Cell suspensions were loaded onto the
570 Chromium Controller, aiming for recovery of 10,000 cells per sample. Libraries were generated
571 using the Chromium Next GEM Single Cell 3′ v3.1 (10x Genomics), according to
572 manufacturer's instructions, and sequenced as 150-bp paired-end reads on an Illumina NovaSeq
573 6000 system with an S4 flow cell.

574

575 *Analysis of 10x Genomics scRNA-seq data*

576 Alignment, filtering, barcode counting, and UMI counting were done via *count* function in Cell
577 Ranger v.4.0.0 with default settings using Cell Ranger's mm10-2020-A reference package (i.e.,
578 the GRCm38/mm10 mouse genome assembly with GENCODE vM23/Ensembl 98 annotation).
579 Using Seurat v.3.2.3 (Stuart et al., 2019), cells were filtered for less than 10% mitochondrial
580 reads, more than 1000 detected features, and a doublet score (generated by the *bcds* in scds
581 v.1.2.0) of less than 0.4. Using protein-coding genes, UMI counts from both wild-type and
582 *Meioc*-null samples were integrated and clusters identified using the first 30 dimensions.
583 The wild-type samples were used to assign cell types to clusters. Five somatic cell types
584 were identified based on cell type-enriched gene expression: fetal Leydig cells (*Dlk1*, *Cyp11a1*)
585 (Kaftanovskaya et al., 2015; Ye et al., 2017), peritubular myoid cells (*Acta2*, *Myh11*) (Chen et
586 al., 2016; Cool et al., 2008), vascular endothelium (*Tm4sf1*) (Shih et al., 2009), testicular
587 macrophages (*Cd14*, *Adgre1*, *Itgam*) (Bhushan et al., 2020; Landmann et al., 2000), and Sertoli
588 cells (*Sox9*, *Cldn11*) (Mazaud-Guittot et al., 2010; Sekido et al., 2004). Germ cells were
589 identified via *Ddx4* and *Dazl*. Then, using additional cell type-enriched gene expression along
590 with UMAP-based cluster relationships, subclusters of spermatogenic cells were assigned to the
591 following cell types: spermatogonial stem cells (*Id4*, *Gfra1*, *Etv5*) (He et al., 2007; Helsel et al.,
592 2017; Sun et al., 2015; Wu et al., 2011), undifferentiated spermatogonia (*Zbtb16*) (Hobbs et al.,
593 2012), type A spermatogonia (*Kit*, *Stra8*, *Ccnd2*) (Beumer et al., 2000; Endo et al., 2015;
594 Schrans-Stassen et al., 1999; Yoshinaga et al., 1991), intermediate/type B spermatogonia (*Kit*)
595 (Schrans-Stassen et al., 1999; Yoshinaga et al., 1991), preleptotene spermatocytes (*Stra8*),
596 leptotene and zygotene spermatocytes (*Meiob*) (Chen et al., 2018; Souquet et al., 2013), and
597 pachytene spermatocytes (*Piwil1*) (Chen et al., 2018; Deng and Lin, 2002).
598 Spermatogenic clusters were further refined based on cell cycle phase using the
599 *CellCycleScoring* function in Seurat to identify type B spermatogonia in G2/M phase, as well as
600 preleptotene spermatocytes in G1, early S, and late S phases (Fig. S1C,D). Clusters were merged
601 as needed. Cell cycle designations of the preleptotene clusters were confirmed via gene
602 expression patterns in wild-type cells independent of the gene:cell cycle phase pairings used by
603 Seurat's *CellCycleScoring* function (Fig. S3). These final cell type designations were then
604 applied to the *Meioc*-null samples. The Mutant-only (Mut) cluster was primarily composed of
605 *Meioc*-null spermatocyte cells, and only four wild-type germ cells were assigned to this cluster.
606 The assignment of the 4 wild-type cells to the Mut cluster was considered to be a scRNA-seq

607 artifact and these cells were excluded from subsequent analysis.

608 In addition to the somatic and germ cell clusters shown in Fig. S1A,B, one additional
609 somatic cell cluster and one additional germ cell cluster were identified but could not be assigned
610 a cell type using marker expression. This unassigned germ cell cluster is likely a technical
611 artifact as it exhibits a median number of features lower than that of all other assigned germ cell
612 subpopulations (Fig. S2A). The unassigned somatic and germ cell clusters, along with all other
613 somatic clusters, were excluded from subsequent analyses. See Supplementary Materials and
614 Methods for additional details on cluster-specific enrichment or depletion in wild-type cells and
615 Gene Set Enrichment Analysis (GSEA).

616 Pseudotime trajectories were built in Monocle 3 v1.0.0 (Qiu et al., 2017a; Qiu et al.,
617 2017b; Trapnell et al., 2014) using the following procedure: the Seurat object containing germ
618 cell clusters only was imported as a Monocle object; data were normalized and pre-processed
619 (function *preprocess_cds()*; options: num_dim = 100); batch effects were removed (function
620 *align_cds()*; options: alignment_group = "batch"); dimensionality reduction was done via UMAP
621 (function *reduce_dimension()*); cells were clustered (function *cluster_cells()*); a principal graph
622 was learned from the reduced dimension space (function *learn_graph()*); and cells were ordered
623 by selecting the Undiff cluster as the starting branch of the trajectory (function *order_cells()*).
624 Cluster cell-type assignments made in Seurat were maintained in the pseudotime trajectories.

625 For differential expression analysis between wild-type and *Meioc*-null germ cells, $\log_2$
626 fold change was defined as wild-type over *Meioc*-null germ cells, such that the value reflects
627 MEIOC's activity in the unperturbed wild-type state. Differential expression analysis of scRNA-
628 seq data was done on each germ cell cluster on genes with a minimum absolute $\log_2$ fold change
629 of 0.1 and that were detected in at least 25% of either population using Seurat's *FindMarkers*
630 function (options: logfc.threshold = 0.1, min.pct = 0.25); *P* values were adjusted for multiple
631 hypothesis testing of tested genes across all nine germ cell clusters via the Bonferroni correction
632 using the *p.adjust* function in R. Additional expressed genes (i.e., genes detected in at least 25%
633 of cells in wild-type or *Meioc*-null cells per cluster) that failed to meet the $\log_2$ fold change
634 threshold for differential expression testing were identified via the *FindMarkers* function
635 (options: logfc.threshold=0, min.pct = 0.25), and their *P* values were marked as "nd" for
636 differential expression testing "not done." See Supplementary Material and Methods for

637 additional details on Gene Ontology analysis, cell cycle analysis of differentially expressed
638 genes, and de novo motif analysis.
639 Dot plots were generated using Seurat's *DotPlot* function with parameter scale=FALSE
640 to maintain average expression from wild-type and *Meioc*-null samples on the same scale.
641
642 *Synchronization of spermatogenesis*
643 Spermatogenesis was synchronized using a protocol originally developed by Hogarth et al.
644 (Hogarth et al., 2013) and modified by Romer et al. (Romer et al., 2018). See Supplementary
645 Material and Methods for details.
646
647 *Bulk RNA-seq analysis of preleptotene-enriched testes*
648 Total RNA was extracted from four wild-type samples and three *Meioc*-null samples, using 1.5
649 synchronized testes from a single pup per sample. TRIzol Reagent (Thermo Fisher Scientific)
650 was added to freshly thawed whole testes, and ERCC RNA ExFold RNA Spike-In Mix 1 and 2
651 (Thermo Fisher Scientific) were added to wild-type and *Meioc*-null samples, respectively, at a
652 concentration of 1 μl of a 1:100 dilution of spike-in mix per 1 mg of testis tissue. (Spike-in mixes
653 were ultimately not used for data analysis.) Total RNA was then isolated with chloroform
654 following the manufacturer's protocol, precipitated via isopropanol, and resuspended in RNase-
655 free water. RNA-seq libraries were prepared with the TruSeq Stranded Total RNA kit with the
656 Ribo-Zero Gold rRNA Removal kit. The barcoded libraries were pooled and sequenced with 50-
657 bp single-end reads on an Illumina HiSeq 2500 machine.
658 Reads were quality trimmed using cutadapt v1.8 (options: -q 30 --minimum-length 20 -b
659 AGATCGGAAGAGC). Expression levels of all transcripts in the mouse Gencode Basic vM15
660 gene annotation were estimated using kallisto v0.44.0 (Bray et al., 2016) with sequence-bias
661 correction (--bias) and strand-specific pseudoalignment (--rf-stranded). Quantified transcripts
662 were filtered for protein-coding genes, transcript-level estimated counts and transcripts per
663 million (TPM) values were summed to the gene level, and TPMs were renormalized to
664 transcript-per-million units.
665 To identify the MEIOC-dependent differential expression program, read counts from
666 kallisto were rounded to the nearest integer and then supplied to DESeq2 v1.26.0 (Love et al.,
667 2014). Genes were filtered for a minimum TPM of 1 in at least three of seven 2S preleptotene

668 samples. Differential expression was defined using a cutoff of adjusted *P* value < 0.05. See
669 Supplementary Material and Methods for additional details on cell cycle analysis, Gene
670 Ontology analysis, and de novo motif analysis.
671 For analysis of transcript stability and transcriptional rates, reads were mapped to the
672 mouse genome (mm10) with the GENCODE Basic vM15 gene annotation via STAR v2.7.1a
673 (Dobin et al., 2013) (options: --outFilterMultimapNmax 1 --alignEndsType Extend5pOfRead1 --
674 outFilterMismatchNmax 2 --outSAMattributes None). All other parameters were set to default.
675 Counts were quantified by htseq v0.11.0 (options: -m union --stranded=reverse) at the gene level
676 (-type gene) and exon level (-type exon), and intron levels were calculated as gene-level counts
677 minus exon-level counts. Changes in transcript stability, transcriptional rate, and abundance were
678 calculated for each gene for each sample using REMBRANDTS (Alkallas et al., 2017) with a
679 stringency of 0.80 and linear bias mode.
680 The cumulative distribution of the $\log_2$ fold change (WT/*Meioc* KO) in transcript stability
681 or transcriptional rate in MEIOC-upregulated or -downregulated transcripts was compared to
682 expressed but unchanged transcripts via a two-tailed Wilcoxon rank sum test with Bonferroni
683 correction for multiple hypothesis testing using the *wilcox.test* and *p.adjust* functions in R.
684 MEIOC-upregulated genes were defined as $\log_2$ fold change WT/*Meioc* KO > 0 and $P < 0.05$
685 and MEIOC-downregulated genes were defined as $\log_2$ fold change WT/*Meioc* KO < 0 and $P <$
686 0.05 based on the DESeq2 analysis of the bulk RNA-seq data.
687
688 *Re-analysis of STRA8 RNA-seq dataset*
689 RNA-seq data from *Stra8*-null and *Stra8*-heterozygote (i.e., phenotypically wild-type)
690 preleptotene spermatocytes (NCBI GEO GSE115928; Kojima et al., 2019) were reanalyzed.
691 Genes with STRA8-bound promoters identified by ChIP-seq in testes enriched for preleptotene
692 spermatocytes were extracted from Supplementary File 2 (Kojima et al. 2019)
693 (https://doi.org/10.7554/eLife.43738.028). See Supplementary Material and Methods for details.
694
695 *Re-analysis of MEIOC RIP-seq dataset and comparison to YTHDC2 and RBM46 CLIP datasets*
696 MEIOC RIP-seq from P15 testes (NCBI GEO GSE96920; Soh et al., 2017) were reanalyzed,
697 with additional details in Supplementary Material and Methods.

698 YTHDC2-bound mRNAs identified via CLIP-seq in P8 and P10 testes were extracted
699 from Tables S1 and S2 (Saito et al., 2022)
700 (http://genesdev.cshlp.org/content/suppl/2022/01/19/gad.349190.121.DC1/Supplemental_Tables.
701 xlsx).
702 RBM46 eCLIP data from P12-P14 testes (NCBI GEO GSE197282) (Qian et al., 2022)
703 were reanalyzed, with additional details in Supplementary Material and Methods.
704
705 *Identification of transcriptional repressors that are repressed by MEIOC-YTHDC2-RBM46*
706 To identify transcriptional repressors that are repressed by MEIOC-YTHDC2-RBM46, we first
707 identified transcripts that were (i) downregulated by MEIOC in the In/B, B G2M, and/or pL G1
708 clusters and (ii) targeted by MEIOC-YTHDC2-RBM46. We then manually examined the
709 "Function" description of the UniProtKB database (release 2020_01; www.uniprot.org) for these
710 mouse proteins. Any proteins that were annotated as repressing transcription or gene expression
711 were considered transcriptional repressors.
712
713 *Re-analysis of E2F6 and MGA ChIP-seq datasets and RNA-seq datasets from ESCs*
714 The following datasets were reanalyzed here: E2F6 ChIP-seq and input data from wild-type and
715 *E2f6*-knockout mouse ESCs (NCBI GEO GSE149025) (Dahlet et al., 2021); MGA and IgG
716 ChIP-seq from wild-type mouse ESCs (ArrayExpress E-MTAB-6007) (Stielow et al., 2018);
717 mouse ESC RNA-seq data from wild-type and *E2f6*-knockout samples (NCBI GEO
718 GSE149025) (Dahlet et al., 2021); and wild-type and *Mga*-knockout samples (NCBI GEO
719 GSE144141) (Qin et al., 2021). See supplementary Material and Methods for details.
720
721 *Immunostaining*
722 Immunostaining was carried out in tissue sections using the following primary antibodies: anti-
723 DMRT1 (Santa Cruz Biotechnology sc-377167, 1:200 dilution for fluorescent staining); anti-
724 MEIOSIN (guinea pig polyclonal from Ishiguro et al., 2020, 1:100 dilution for fluorescent
725 staining); anti-STRA8 (Abcam ab49405, 1:500 dilution for chromogenic staining or 1:200 for
726 fluorescent staining); and anti-STRA8 (Abcam ab49602, 1:200 dilution for fluorescent staining).
727 See supplementary Material and Methods for details.
728

Competing Interest Statement

The authors declare no competing interests.

Acknowledgements

We thank Kei-Ichiro Ishiguro for the MEIOSIN antibody; Mary Goodheart, Mina Kojima, Holly Christensen, and Peter Nicholls for technical help; and Abigail Groff and Linyong Mao for advice on bioinformatics analysis. We are grateful to the members of the Page Lab for valuable feedback, and to Winston Bellott, Jordana Bloom, ZY Chen, Jennifer Hughes, Mina Kojima, and Adrianna San Roman for comments on the manuscript.

We thank the Whitehead Genome Technology Core for library preparation and Illumina sequencing, and the Whitehead Institute FACS Facility for cell sorting. Fluorescent microscopy was done at the Whitehead Institute's WM Keck Foundation Biological Imaging Facility and Cincinnati Children's Bio-Imaging and Analysis Facility (RRID:SCR_022628).

Competing Interests Statement

No competing interests declared.

Funding

This work was supported by the Eunice Kennedy Shriver National Institute of Child Health and Human Development of the National Institutes of Health under Award Numbers F32HD093391 (M.M.M), K99HD097285 (M.M.M), and R00HD097285 (M.M.M), and by the Howard Hughes Medical Institute, where D.C.P. is an Investigator.

Author Contributions

M.M.M and B.L. prepared samples for 10x Genomic analysis. D.deR. assessed germ cell stage in synchronized testis samples. M.M.M. and N.G.P. carried out immunostaining experiments. M.M.M. performed all other experiments and data analysis. M.M.M. and D.C.P. designed the study and wrote the manuscript with contributions from all authors.

Data availability

759 Sequencing data have been deposited to the Gene Expression Omnibus under accession number
760 GSE230747.
761

762 **REFERENCES**

763 Abby, E., Tourpin, S., Ribeiro, J., Daniel, K., Messiaen, S., Moison, D., Guerquin, J., Gaillard,
764 J.-C., Armengaud, J., Langa, F., et al. (2016). Implementation of meiosis prophase I
765 programme requires a conserved retinoid-independent stabilizer of meiotic transcripts.
766 *Nat. Commun.* 7, 10324.

767 Alkallas, R., Fish, L., Goodarzi, H. and Najafabadi, H. S. (2017). Inference of RNA decay rate
768 from transcriptional profiling highlights the regulatory programs of Alzheimer's disease.
769 *Nat. Commun.* 8, 909.

770 Anderson, E. L., Baltus, A. E., Roepers-Gajadien, H. L., Hassold, T. J., de Rooij, D. G., van Pelt,
771 A. M. M. and Page, D. C. (2008). Stra8 and its inducer, retinoic acid, regulate meiotic
772 initiation in both spermatogenesis and oogenesis in mice. *Proc. Natl. Acad. Sci. U. S. A.*
773 105, 14976–14980.

774 Bailey, A. S., Batista, P. J., Gold, R. S., Chen, Y. G., de Rooij, D. G., Chang, H. Y. and Fuller,
775 M. T. (2017). The conserved RNA helicase YTHDC2 regulates the transition from
776 proliferation to differentiation in the germline. *eLife* 6,.

777 Baltus, A. E., Menke, D. B., Hu, Y.-C., Goodheart, M. L., Carpenter, A. E., de Rooij, D. G. and
778 Page, D. C. (2006). In germ cells of mouse embryonic ovaries, the decision to enter
779 meiosis precedes premeiotic DNA replication. *Nat. Genet.* 38, 1430–1434.

780 Beumer, T. L., Roepers-Gajadien, H. L., Gademan, I. S., Kal, H. B. and de Rooij, D. G. (2000).
781 Involvement of the D-type cyclins in germ cell proliferation and differentiation in the
782 mouse. *Biol. Reprod.* 63, 1893–8.

783 Bhushan, S., Theas, M. S., Guazzone, V. A., Jacobo, P., Wang, M., Fijak, M., Meinhardt, A. and
784 Lustig, L. (2020). Immune cell subtypes and their function in the testis. *Front. Immunol.*
785 11, 2558.

786 Bray, N. L., Pimentel, H., Melsted, P. and Pachter, L. (2016). Near-optimal probabilistic RNA-
787 seq quantification. *Nat. Biotechnol.* 34, 525–527.

788 Burn, S. F., Washkowitz, A. J., Gavrilov, S. and Papaioannou, V. E. (2018). Postimplantation
789 Mga expression and embryonic lethality of two gene-trap alleles. *Gene Expr. Patterns*
790 *GEP* 27, 31–35.

791 Chen, D., Wu, C., Zhao, S., Geng, Q., Gao, Y., Li, X., Zhang, Y. and Wang, Z. (2014). Three
792 RNA binding proteins form a complex to promote differentiation of germline stem cell
793 lineage in Drosophila. *PLoS Genet.* 10, e1004797.

794 Chen, L.-Y., Willis, W. D. and Eddy, E. M. (2016). Targeting the Gdnf gene in peritubular
795 myoid cells disrupts undifferentiated spermatogonial cell development. *Proc. Natl. Acad.*
796 *Sci. U. S. A.* 113, 1829–34.

797 Chen, Y., Zheng, Y., Gao, Y., Lin, Z., Yang, S., Wang, T., Wang, Q., Xie, N., Hua, R., Liu, M.,
798 et al. (2018). Single-cell RNA-seq uncovers dynamic processes and critical regulators in
799 mouse spermatogenesis. *Cell Res.* 28, 879–896.

800 Cool, J., Carmona, F. D., Szucsik, J. C. and Capel, B. (2008). Peritubular myoid cells are not the
801 migrating population required for testis cord formation in the XY gonad. *Sex. Dev. Genet.*
802 *Mol. Biol. Evol. Endocrinol. Embryol. Pathol. Sex Determ. Differ.* 2, 128–33.

803 Dahlet, T., Truss, M., Frede, U., Al Adhami, H., Bardet, A. F., Dumas, M., Vallet, J., Chicher, J.,
804 Hammann, P., Kottnik, S., et al. (2021). E2F6 initiates stable epigenetic silencing of
805 germline genes during embryonic development. *Nat. Commun.* 12, 3582.

806 Deng, W. and Lin, H. (2002). miwi, a murine homolog of piwi, encodes a cytoplasmic protein
807 essential for spermatogenesis. *Dev. Cell* 2, 819–30.

808 Dix, D. J., Allen, J. W., Collins, B. W., Mori, C., Nakamura, N., Poorman-Allen, P., Goulding,
809 E. H. and Eddy, E. M. (1996). Targeted gene disruption of Hsp70-2 results in failed
810 meiosis, germ cell apoptosis, and male infertility. *Proc. Natl. Acad. Sci. U. S. A.* 93,
811 3264–3268.

812 Dobin, A., Davis, C. A., Schlesinger, F., Drenkow, J., Zaleski, C., Jha, S., Batut, P., Chaisson,
813 M. and Gingeras, T. R. (2013). STAR: Ultrafast universal RNA-seq aligner.
814 *Bioinformatics* 29, 15–21.

815 Dokshin, G. A., Baltus, A. E., Eppig, J. J. and Page, D. C. (2013). Oocyte differentiation is
816 genetically dissociable from meiosis in mice. *Nat. Genet.* 45, 877–883.

817 Endo, T., Romer, K. A., Anderson, E. L., Baltus, A. E., de Rooij, D. G. and Page, D. C. (2015).
818 Periodic retinoic acid-STRA8 signaling intersects with periodic germ-cell competencies
819 to regulate spermatogenesis. *Proc. Natl. Acad. Sci. U. S. A.* 112, E2347-56.

820 Endo, T., Mikedis, M. M., Nicholls, P. K., Page, D. C. and de Rooij, D. G. (2019). Retinoic acid
821 and germ cell development in the ovary and testis. *Biomolecules* 9,.

822 Gaidatzis, D., Burger, L. and Stadler, M. B. (2015). Analysis of intronic and exonic reads in
823 RNA-seq data characterizes transcriptional and post-transcriptional regulation. *Nat.*
824 *Biotechnol.* 33, 722–9.

825 Gonczy, P., Matunis, E. and DiNardo, S. (1997). bag-of-marbles and benign gonial cell
826 neoplasm act in the germline to restrict proliferation during Drosophila spermatogenesis.
827 *Development* 124, 4361–4371.

828 He, Z., Jiang, J., Hofmann, M.-C. and Dym, M. (2007). Gfra1 silencing in mouse spermatogonial
829 stem cells results in their differentiation via the inactivation of RET tyrosine kinase. *Biol.*
830 *Reprod.* 77, 723–33.

831 Helsel, A. R., Yang, Q.-E., Oatley, M. J., Lord, T., Sablitzky, F. and Oatley, J. M. (2017). ID4
832 levels dictate the stem cell state in mouse spermatogonia. *Development* 144, 624–634.

833 Hobbs, R. M., Fagoonee, S., Papa, A., Webster, K., Altruda, F., Nishinakamura, R., Chai, L. and
834 Pandolfi, P. P. (2012). Functional antagonism between Sall4 and Plzf defines germline
835 progenitors. *Cell Stem Cell* 10, 284–298.

836 Hogarth, C. A., Evanoff, R., Mitchell, D., Kent, T., Small, C., Amory, J. K. and Griswold, M. D.
837 (2013). Turning a spermatogenic wave into a tsunami: synchronizing murine
838 spermatogenesis using WIN 18,446. *Biol. Reprod.* 88, 1–9.

839 Hsiao, C. J., Tung, P., Blischak, J. D., Burnett, J. E., Barr, K. A., Dey, K. K., Stephens, M. and
840 Gilad, Y. (2020). Characterizing and inferring quantitative cell cycle phase in single-cell
841 RNA-seq data analysis. *Genome Res.* 30, 611–621.

842 Hsu, P. J., Zhu, Y., Ma, H., Guo, Y., Shi, X., Liu, Y., Qi, M., Lu, Z., Shi, H., Wang, J., et al.
843 (2017). Ythdc2 is an N6-methyladenosine binding protein that regulates mammalian
844 spermatogenesis. *Cell Res.* 27, 1115–1127.

845 Insco, M. L., Leon, A., Tam, C. H., McKearin, D. M. and Fuller, M. T. (2009). Accumulation of
846 a differentiation regulator specifies transit amplifying division number in an adult stem
847 cell lineage. *Proc. Natl. Acad. Sci. U. S. A.* 106, 22311–6.

848 Insco, M. L., Bailey, A. S., Kim, J., Olivares, G. H., Wapinski, O. L., Tam, C. H. and Fuller, M.
849 T. (2012). A Self-Limiting Switch Based on Translational Control Regulates the
850 Transition from Proliferation to Differentiation in an Adult Stem Cell Lineage. *Cell Stem*
851 *Cell* 11, 689–700.

852 Ishiguro, K. ichiro, Matsuura, K., Tani, N., Takeda, N., Usuki, S., Yamane, M., Sugimoto, M.,
853 Fujimura, S., Hosokawa, M., Chuma, S., et al. (2020a). MEIOSIN directs the switch from
854 mitosis to meiosis in mammalian germ cells. *Dev. Cell* 52, 429-445.e10.

855 Ishiguro, K. ichiro, Matsuura, K., Tani, N., Takeda, N., Usuki, S., Yamane, M., Sugimoto, M.,
856 Fujimura, S., Hosokawa, M., Chuma, S., et al. (2020b). MEIOSIN Directs the Switch
857 from Mitosis to Meiosis in Mammalian Germ Cells. *Dev. Cell* 52, 429-445.e10.

858 Jain, D., Puno, M. R., Meydan, C., Lailler, N., Mason, C. E., Lima, C. D., Anderson, K. V. and
859 Keeney, S. (2018). ketu mutant mice uncover an essential meiotic function for the ancient
860 RNA helicase YTHDC2. *eLife* 7,.

861 Johnson, T. A., Niedenberger, B. A., Kirsanov, O., Harrington, E. V., Malachowski, T. and
862 Geyer, C. B. (2023). Differential responsiveness of spermatogonia to retinoic acid
863 dictates precocious differentiation but not meiotic entry during steady-state
864 spermatogenesis. *Biol. Reprod.* 108, 822–836.

865 Kaftanovskaya, E. M., Lopez, C., Ferguson, L., Myhr, C. and Agoulnik, A. I. (2015). Genetic
866 ablation of androgen receptor signaling in fetal Leydig cell lineage affects Leydig cell
867 functions in adult testis. *FASEB J. Off. Publ. Fed. Am. Soc. Exp. Biol.* 29, 2327–37.

868 Kassir, Y., Granot, D. and Simchen, G. (1988). IME1, a positive regulator gene of meiosis in S.
869 cerevisiae. *Cell* 52, 853–862.

870 Kehoe, S. M., Oka, M., Hankowski, K. E., Reichert, N., Garcia, S., McCarrey, J. R., Gaubatz, S.
871 and Terada, N. (2008). A conserved E2F6-binding element in murine meiosis-specific
872 gene Promoters. *Biol. Reprod.* 79, 921–930.

873 Kimble, J. (2011). Molecular regulation of the mitosis/meiosis decision in multicellular
874 organisms. *Cold Spring Harb. Perspect. Biol.* 3, a002683.

875 Kitamura, Y., Uranishi, K., Hirasaki, M., Nishimoto, M., Suzuki, A. and Okuda, A. (2021).
876 Identification of germ cell-specific Mga variant mRNA that promotes meiosis via
877 impediment of a non-canonical PRC1. *Sci. Rep.* 11, 9737.

878 Kojima, M. L., de Rooij, D. G. and Page, D. C. (2019). Amplification of a broad transcriptional
879 program by a common factor triggers the meiotic cell cycle in mice. *eLife* 8,.

880 Koubova, J., Hu, Y.-C., Bhattacharyya, T., Soh, Y. Q. S., Gill, M. E., Goodheart, M. L., Hogarth,
881 C. a, Griswold, M. D. and Page, D. C. (2014). Retinoic acid activates two pathways
882 required for meiosis in mice. *PLoS Genet.* 10, e1004541.

883 Kretschmer, J., Rao, H., Hackert, P., Sloan, K. E., Höbartner, C. and Bohnsack, M. T. (2018).
884 The m6A reader protein YTHDC2 interacts with the small ribosomal subunit and the 5'-
885 3' exoribonuclease XRN1. *RNA N. Y. N* 24, 1339–1350.

886 Landmann, R., Müller, B. and Zimmerli, W. (2000). CD14, new aspects of ligand and signal
887 diversity. *Microbes Infect.* 2, 295–304.

888 Li, L., Krasnykov, K., Homolka, D., Gos, P., Mendel, M., Fish, R. J., Pandey, R. R. and Pillai, R.
889 S. (2022). The XRN1-regulated RNA helicase activity of YTHDC2 ensures mouse
890 fertility independently of m6A recognition. *Mol. Cell* 82, 1678-1690.e12.

891 Love, M. I., Huber, W. and Anders, S. (2014). Moderated estimation of fold change and
892 dispersion for RNA-seq data with DESeq2. *Genome Biol.* 15, 550.

893 Madisen, L., Zwingman, T. A., Sunkin, S. M., Oh, S. W., Zariwala, H. A., Gu, H., Ng, L. L.,
894 Palmiter, R. D., Hawrylycz, M. J., Jones, A. R., et al. (2010). A robust and high-
895 throughput Cre reporting and characterization system for the whole mouse brain. *Nat.*
896 *Neurosci.* 13, 133–140.

897 Maeda, I., Okamura, D., Tokitake, Y., Ikeda, M., Kawaguchi, H., Mise, N., Abe, K., Noce, T.,
898 Okuda, A. and Matsui, Y. (2013). Max is a repressor of germ cell-related gene expression
899 in mouse embryonic stem cells. *Nat. Commun.* 4, 1754.

900 Mark, M., Jacobs, H., Oulad-Abdelghani, M., Dennefeld, C., Féret, B., Vernet, N., Codreanu, C.-
901 A., Chambon, P. and Ghyselinck, N. B. (2008). STRA8-deficient spermatocytes initiate,
902 but fail to complete, meiosis and undergo premature chromosome condensation. *J. Cell*
903 *Sci.* 121, 3233–3242.

904 Matson, C. K., Murphy, M. W., Griswold, M. D., Yoshida, S., Bardwell, V. J. and Zarkower, D.
905 (2010). The mammalian doublesex homolog DMRT1 Is a transcriptional gatekeeper that
906 controls the mitosis versus meiosis decision in male germ cells. *Dev. Cell* 19, 612–624.

907 Mazaud-Guittot, S., Meugnier, E., Pesenti, S., Wu, X., Vidal, H., Gow, A. and Le Magueresse-
908 Battistoni, B. (2010). Claudin 11 deficiency in mice results in loss of the Sertoli cell
909 epithelial phenotype in the testis. *Biol. Reprod.* 82, 202–13.

910 McKearin, D. M. and Spradling, A. C. (1990). bag-of-marbles: a Drosophila gene required to
911 initiate both male and female gametogenesis. *Genes Dev.* 4, 2242–51.

912 Nakagawa, T., Zhang, T., Kushi, R., Nakano, S., Endo, T., Nakagawa, M., Yanagihara, N.,
913 Zarkower, D. and Nakayama, K. (2017). Regulation of mitosis-meiosis transition by the
914 ubiquitin ligase β-TrCP in male germ cells. *Dev. Camb. Engl.* 144, 4137–4147.

915 Ostapcuk, V., Mohn, F., Carl, S. H., Basters, A., Hess, D., Iesmantavicius, V., Lampersberger,
916 L., Flemr, M., Pandey, A., Thomä, N. H., et al. (2018). Activity-dependent
917 neuroprotective protein recruits HP1 and CHD4 to control lineage-specifying genes.
918 *Nature* 557, 739–743.

919 Peart, N. J., Johnson, T. A., Lee, S., Sears, M. J., Yang, F., Quesnel-Vallières, M., Feng, H.,
920 Recinos, Y., Barash, Y., Zhang, C., et al. (2022). The germ cell-specific RNA binding
921 protein RBM46 is essential for spermatogonial differentiation in mice. *PLoS Genet.* 18,
922 e1010416.

923 Pohlers, M., Truss, M., Frede, U., Scholz, A., Strehle, M., Kuban, R.-J., Hoffmann, B., Morkel,
924 M., Birchmeier, C. and Hagemeier, C. (2005). A Role for E2F6 in the Restriction of
925 Male-Germ-Cell-Specific Gene Expression. *Curr. Biol.* 15, 1051–1057.

926 Qian, B., Li, Y., Yan, R., Han, S., Bu, Z., Gong, J., Zheng, B., Yuan, Z., Ren, S., He, Q., et al.
927 (2022). RNA binding protein RBM46 regulates mitotic-to-meiotic transition in
928 spermatogenesis. *Sci. Adv.* 8, eabq2945.

929 Qin, J., Wang, C., Zhu, Y., Su, T., Dong, L., Huang, Y. and Hao, K. (2021). Mga safeguards
930 embryonic stem cells from acquiring extraembryonic endoderm fates. *Sci. Adv.* 7,
931 eabe5689.

932 Qiu, X., Hill, A., Packer, J., Lin, D., Ma, Y.-A. and Trapnell, C. (2017a). Single-cell mRNA
933 quantification and differential analysis with Census. *Nat. Methods* 14, 309–315.

934 Qiu, X., Mao, Q., Tang, Y., Wang, L., Chawla, R., Pliner, H. A. and Trapnell, C. (2017b).
935 Reversed graph embedding resolves complex single-cell trajectories. *Nat. Methods* 14,
936 979–982.

937 Romer, K. A., de Rooij, D. G., Kojima, M. L. and Page, D. C. (2018). Isolating mitotic and
938 meiotic germ cells from male mice by developmental synchronization, staging, and
939 sorting. *Dev. Biol.* 443, 19–34.

940 Saito, Y., Hawley, B. R., Puno, M. R., Sarathy, S. N., Lima, C. D., Jaffrey, S. R., Darnell, R. B.,
941 Keeney, S. and Jain, D. (2022). YTHDC2 control of gametogenesis requires helicase
942 activity but not m6A binding. *Genes Dev.* 36, 180–194.

943 Schrans-Stassen, B. H., van de Kant, H. J., de Rooij, D. G. and van Pelt, A. M. (1999).
944 Differential expression of c-kit in mouse undifferentiated and differentiating type A
945 spermatogonia. *Endocrinology* 140, 5894–900.

946 Sekido, R., Bar, I., Narváez, V., Penny, G. and Lovell-Badge, R. (2004). SOX9 is up-regulated
947 by the transient expression of SRY specifically in Sertoli cell precursors. *Dev. Biol.* 274,
948 271–9.

949 Shih, S.-C., Zukauskas, A., Li, D., Liu, G., Ang, L.-H., Nagy, J. A., Brown, L. F. and Dvorak, H.
950 F. (2009). The L6 protein TM4SF1 is critical for endothelial cell function and tumor
951 angiogenesis. *Cancer Res.* 69, 3272–7.

952 Shimada, R., Kato, Y., Takeda, N., Fujimura, S., Yasunaga, K.-I., Usuki, S., Niwa, H., Araki, K.
953 and Ishiguro, K.-I. (2023). STRA8-RB interaction is required for timely entry of meiosis
954 in mouse female germ cells. *Nat. Commun.* 14, 6443.

955 Smith, H. E., Su, S. S., Neigeborn, L., Driscoll, S. E. and Mitchell, A. P. (1990). Role of IME1
956 expression in regulation of meiosis in Saccharomyces cerevisiae. *Mol. Cell. Biol.* 10,
957 6103–6113.

958 Soh, Y. Q. S., Junker, J. P., Gill, M. E., Mueller, J. L., van Oudenaarden, A. and Page, D. C.
959 (2015). A Gene Regulatory Program for Meiotic Prophase in the Fetal Ovary. *PLoS*
960 *Genet.* 11, e1005531.

961 Soh, Y. Q. S., Mikedis, M. M., Kojima, M., Godfrey, A. K., de Rooij, D. G. and Page, D. C.
962 (2017). Meioc maintains an extended meiotic prophase I in mice. *PLoS Genet.* 13,
963 e1006704.

964 Souquet, B., Abby, E., Hervé, R., Finsterbusch, F., Tourpin, S., Le Bouffant, R., Duquenne, C.,
965 Messiaen, S., Martini, E., Bernardino-Sgherri, J., et al. (2013). MEIOB Targets Single-
966 Strand DNA and Is Necessary for Meiotic Recombination. *PLoS Genet.* 9, e1003784.

967 Stielow, B., Finkernagel, F., Stiewe, T., Nist, A. and Suske, G. (2018). MGA, L3MBTL2 and
968 E2F6 determine genomic binding of the non-canonical Polycomb repressive complex
969 PRC1.6. *PLOS Genet.* 14, e1007193.

970 Storre, J., Elsässer, H., Fuchs, M., Ullmann, D., Livingston, D. M. and Gaubatz, S. (2002).
971 Homeotic transformations of the axial skeleton that accompany a targeted deletion of
972 *E2f6*. *EMBO Rep.* 3, 695–700.

973 Stuart, T., Butler, A., Hoffman, P., Hafemeister, C., Papalexi, E., Mauck, W. M., Hao, Y.,
974 Stoeckius, M., Smibert, P. and Satija, R. (2019). Comprehensive integration of single-cell
975 data. *Cell* 177, 1888-1902.e21.

976 Sun, F., Xu, Q., Zhao, D. and Degui Chen, C. (2015). Id4 marks spermatogonial stem cells in the
977 mouse testis. *Sci. Rep.* 5, 17594.

978 Suzuki, A., Hirasaki, M., Hishida, T., Wu, J., Okamura, D., Ueda, A., Nishimoto, M., Nakachi,
979 Y., Mizuno, Y., Okazaki, Y., et al. (2016). Loss of MAX results in meiotic entry in
980 mouse embryonic and germline stem cells. *Nat. Commun.* 7, 11056.

981 Suzuki, A., Uranishi, K., Nishimoto, M., Mizuno, Y., Mizuno, S., Takahashi, S., Eisenman, R.
982 N. and Okuda, A. (2024). MAX controls meiotic entry in sexually undifferentiated germ
983 cells. *Sci. Rep.* 14, 5236.

984 Trapnell, C., Cacchiarelli, D., Grimsby, J., Pokharel, P., Li, S., Morse, M., Lennon, N. J., Livak,
985 K. J., Mikkelsen, T. S. and Rinn, J. L. (2014). The dynamics and regulators of cell fate
986 decisions are revealed by pseudotemporal ordering of single cells. *Nat. Biotechnol.* 32,
987 381–386.

988 Uranishi, K., Hirasaki, M., Kitamura, Y., Mizuno, Y., Nishimoto, M., Suzuki, A. and Okuda, A.
989 (2021). Two DNA binding domains of MGA act in combination to suppress ectopic
990 activation of meiosis-related genes in mouse embryonic stem cells. *Stem Cells* 39, 1435–
991 1446.

992 van Werven, F. J. and Amon, A. (2011). Regulation of entry into gametogenesis. *Philos. Trans.*
993 *R. Soc. B Biol. Sci.* 366, 3521–3531.

994 Washkowitz, A. J., Schall, C., Zhang, K., Wurst, W., Floss, T., Mager, J. and Papaioannou, V. E.
995 (2015). Mga is essential for the survival of pluripotent cells during peri-implantation
996 development. *Dev. Camb. Engl.* 142, 31–40.

997 Wojtas, M. N., Pandey, R. R., Mendel, M., Homolka, D., Sachidanandam, R. and Pillai, R. S.
998 (2017). Regulation of m6A Transcripts by the 3′→5′ RNA Helicase YTHDC2 Is
999 Essential for a Successful Meiotic Program in the Mammalian Germline. *Mol. Cell* 68,
1000 374-387.e12.

1001 Wu, X., Goodyear, S. M., Tobias, J. W., Avarbock, M. R. and Brinster, R. L. (2011).
1002 Spermatogonial stem cell self-renewal requires ETV5-mediated downstream activation of
1003 Brachyury in mice. *Biol. Reprod.* 85, 1114–23.

1004 Ye, L., Li, X., Li, L., Chen, H. and Ge, R.-S. (2017). Insights into the development of the adult
1005 leydig cell lineage from stem leydig cells. *Front. Physiol.* 8, 430.

1006 Yokobayashi, S., Liang, C.-Y., Kohler, H., Nestorov, P., Liu, Z., Vidal, M., van Lohuizen, M.,
1007 Roloff, T. C. and Peters, A. H. F. M. (2013). PRC1 coordinates timing of sexual
1008 differentiation of female primordial germ cells. *Nature* 495, 236–240.

1009 Yoshinaga, K., Nishikawa, S., Ogawa, M., Hayashi, S., Kunisada, T., Fujimoto, T. and
1010 Nishikawa, S. (1991). Role of c-kit in mouse spermatogenesis: identification of
1011 spermatogonia as a specific site of c-kit expression and function. *Development* 113.

1012 Zhang, X., Gunewardena, S. and Wang, N. (2021). Nutrient restriction synergizes with retinoic
1013 acid to induce mammalian meiotic initiation in vitro. *Nat. Commun.* 12, 1758.

1014 Zhang, X., Liu, Y., Sosa, F., Gunewardena, S., Crawford, P. A., Zielen, A. C., Orwig, K. E. and
1015 Wang, N. (2023). Transcriptional metabolic reprogramming implements meiotic fate
1016 decision in mouse testicular germ cells. *Cell Rep.* 42, 112749.

1017

Figure 1

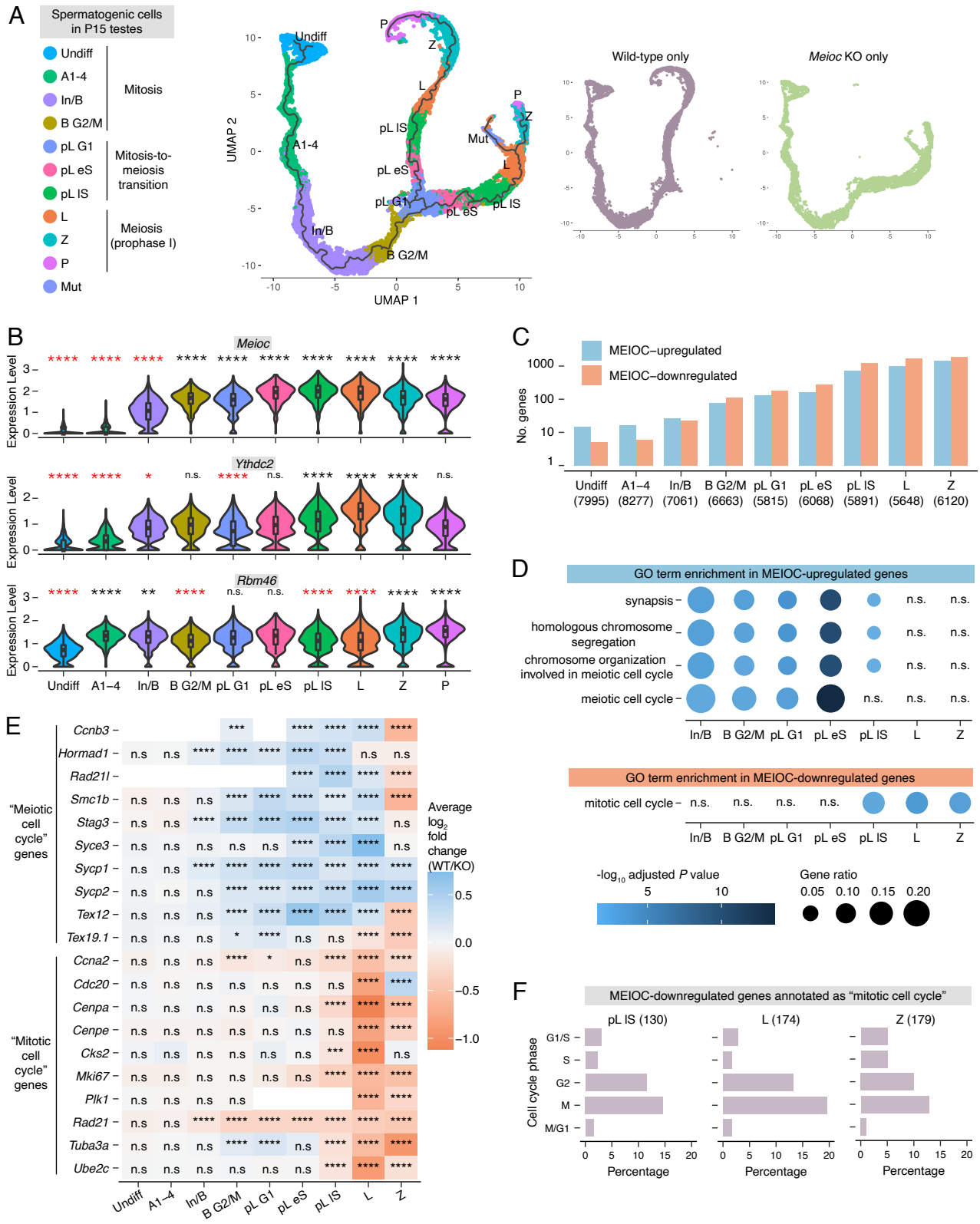
A
Spermatogenic cells in P15 testes
Undiff
A1-4
In/B
B G2/M
pL G1
pL eS
pL lS
L
Z
P
Mut
Mitosis
Mitosis-to-meiosis transition
Meiosis (prophase I)
UMAP 1
UMAP 2
Wild-type only
Meioc KO only
B
Meioc
Ythdc2
Rbm46
Expression Level
Undiff A1–4 In/B B G2/M pL G1 pL eS pL lS L Z P
C
MEIOC–upregulated
MEIOC–downregulated
No. genes
Undiff (7995) A1–4 (8277) In/B (7061) B G2/M (6663) pL G1 (5815) pL eS (6068) pL lS (5891) L (5648) Z (6120)
D
GO term enrichment in MEIOC-upregulated genes
synapsis
homologous chromosome segregation
chromosome organization involved in meiotic cell cycle
meiotic cell cycle
GO term enrichment in MEIOC-downregulated genes
mitotic cell cycle
-log10 adjusted P value
Gene ratio
E
"Meiotic cell cycle" genes
"Mitotic cell cycle" genes
Ccnb3
Hormad1
Rad21l
Smc1b
Stag3
Syce3
Sycp1
Sycp2
Tex12
Tex19.1
Ccna2
Cdc20
Cenpa
Cenpe
Cks2
Mki67
Plk1
Rad21
Tuba3a
Ube2c
Average log2 fold change (WT/KO)
F
MEIOC-downregulated genes annotated as "mitotic cell cycle"
pL lS (130)
L (174)
Z (179)
Cell cycle phase
G1/S
S
G2
M
M/G1
Percentage

1018 **Figure 1: *Meioc*-null germ cells transcriptomically diverge from wild-type germ cells**
1019 **during the G1/S phase transition.**
1020
1021 **A:** UMAP visualization with pseudotime trajectory of wild-type and *Meioc* KO germ cells from
1022 P15 testes. Large plot on left displays both wild-type and *Meioc* KO cells. Smaller plots on right
1023 display cells of a single genotype.
1024 **B:** Expression levels of *Meioc*, *Ythdc2*, and *Rbm46* in germ cell clusters from wild-type testes.
1025 Black and red asterisks designate enrichment or depletion, respectively, relative to all other germ
1026 cells. Clusters marked as "not done" (n.d.) did not meet expression thresholds set for statistical
1027 testing.
1028 **C:** Number of genes identified as MEIOC-upregulated ($\log_2$ fold change (WT/KO)>0.1, adj.
1029 P<0.05) and-downregulated ($\log_2$ fold change (WT/KO)<-0.1, adj. P<0.05) within each germ
1030 cell cluster.
1031 **D:** Gene Ontology (GO) term enrichment analysis for MEIOC-upregulated and -downregulated
1032 genes shown. Graph for MEIOC-upregulated genes displays top 4 enriched categories identified
1033 in the B G2/M cluster. Graph for MEIOC-downregulated genes displays a selected category of
1034 interest.
1035 **E:** Heatmap of $\log_2$ fold changes for selected genes annotated as GO terms "meiotic cell cycle"
1036 or "mitotic cell cycle".
1037 **F:** Associated cell cycle phases for MEIOC-downregulated genes that are annotated as GO term
1038 "mitotic cell cycle." Only those genes whose expression is associated with a specific cell cycle
1039 phase are graphed.
1040
1041 Cluster abbreviations: Undiff, undifferentiated spermatogonia; A1-4, differentiating types A1-A4
1042 spermatogonia; In/B, differentiating Intermediate and type B spermatogonia; B G2M,
1043 differentiating type B spermatogonia in G2/M phase; pL G1, preleptotene spermatocytes in G1
1044 phase; pL eS, preleptotene spermatocytes in early S; pL lS, preleptotene spermatocytes in late S
1045 phase; L, leptotene spermatocytes; Z, zygotene spermatocytes; P, pachytene spermatocytes; Mut,
1046 mutant spermatocytes.
1047
1048 *, adj. P<0.05; **, adj. P<0.01; ***, adj. P<0.001; ****, adj. P<0.0001; n.s., not significant.

Figure 2

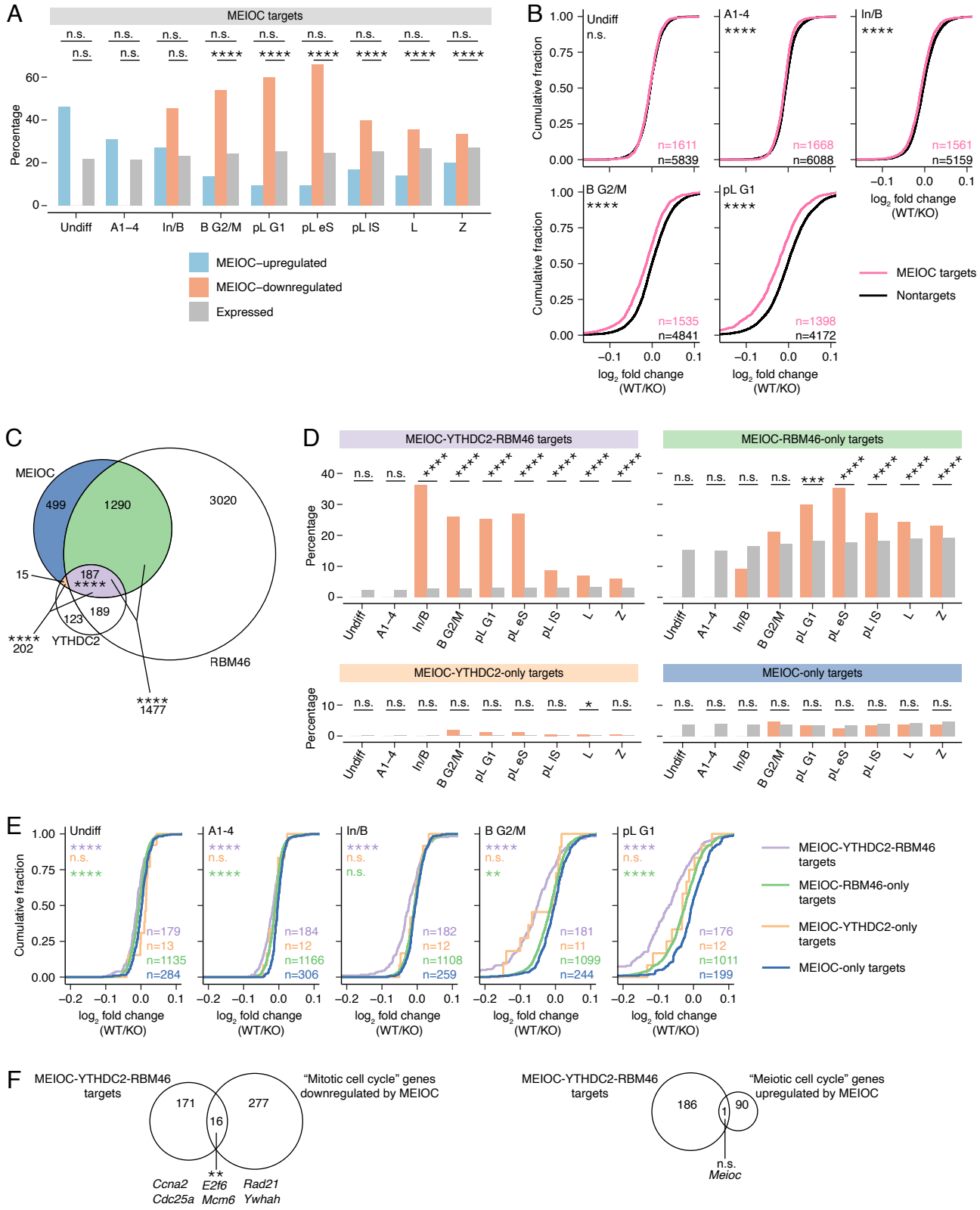
A
MEIOC targets
Percentage
Undiff
A1–4
In/B
B G2/M
pL G1
pL eS
pL lS
L
Z
MEIOC–upregulated
MEIOC–downregulated
Expressed
B
Cumulative fraction
Undiff
A1-4
In/B
B G2/M
pL G1
n=1611
n=5839
n=1668
n=6088
n=1561
n=5159
n=1535
n=4841
n=1398
n=4172
log2 fold change (WT/KO)
MEIOC targets
Nontargets
C
MEIOC
499
1290
3020
15
187
189
123
202
YTHDC2
RBM46
1477
D
MEIOC-YTHDC2-RBM46 targets
MEIOC-RBM46-only targets
MEIOC-YTHDC2-only targets
MEIOC-only targets
Percentage
E
Cumulative fraction
Undiff
A1-4
In/B
B G2/M
pL G1
n=179
n=13
n=1135
n=284
n=184
n=12
n=1166
n=306
n=182
n=12
n=1108
n=259
n=181
n=11
n=1099
n=244
n=176
n=12
n=1011
n=199
log2 fold change (WT/KO)
MEIOC-YTHDC2-RBM46 targets
MEIOC-RBM46-only targets
MEIOC-YTHDC2-only targets
MEIOC-only targets
F
MEIOC-YTHDC2-RBM46 targets
171
16
277
"Mitotic cell cycle" genes downregulated by MEIOC
Ccna2
Cdc25a
E2f6
Mcm6
Rad21
Ywhah
MEIOC-YTHDC2-RBM46 targets
186
1
90
"Meiotic cell cycle" genes upregulated by MEIOC
Meioc

1049 **Figure 2: MEIOC-YTHDC2-RBM46 destabilize their mRNA targets.**

1050

1051 **A:** Percentage of MEIOC targets within MEIOC-upregulated, MEIOC-downregulated, and
1052 expressed genes, defined by scRNA-seq. MEIOC targets were identified from reanalysis of a
1053 published RIP-seq dataset (Soh et al., 2017).
1054 **B:** Cumulative fraction for $\log_2$ fold change (WT / *Meioc* KO), defined by scRNA-seq, with
1055 genes binned as MEIOC targets or nontargets.
1056 **C:** Overlap of mRNAs identified by MEIOC RIP-seq, and YTHDC2 CLIP-seq, and RBM46
1057 eCLIP-seq datasets. MEIOC RIP-seq data were reanalyzed from Soh et al., 2017. YTHDC2
1058 CLIP-seq analysis was published in Saito et al., 2022. RBM46 eCLIP-seq data were reanalyzed
1059 from Qian et al., 2022. Asterisks denote statistical enrichment.
1060 **D:** Percentage of MEIOC-YTHDC2-RBM46 targets, MEIOC-RBM46-only targets, MEIOC
1061 YTHDC2-only targets, and MEIOC-only targets within MEIOC-downregulated and expressed
1062 genes.
1063 **E:** Cumulative fraction for $\log_2$ fold change (WT / *Meioc* KO), defined by scRNA-seq, with
1064 genes binned as MEIOC-YTHDC2-RBM46 targets, MEIOC-RBM46-only targets, MEIOC-
1065 YTHDC2-only targets, and MEIOC-only targets. Asterisks represent comparison of color-
1066 matched target set to MEIOC-only targets.
1067 **F:** MEIOC-YTHDC2-RBM46 targets are enriched for GO term "mitotic cell cycle" genes
1068 downregulated by MEIOC but not GO term "meiotic cell cycle" genes upregulated by MEIOC.
1069 Upregulated and downregulated genes were defined by scRNA-seq (any germ cell cluster).
1070 Asterisks represent statistical enrichment; "n.s." represents "not significant" statistical
1071 enrichment or depletion.

1072

1073 *, adj. $P<0.05$; **, adj. $P<0.01$; ***, adj. $P<0.0001$; ****, adj. $P<0.0001$; n.s., not significant.

1074

Figure 3

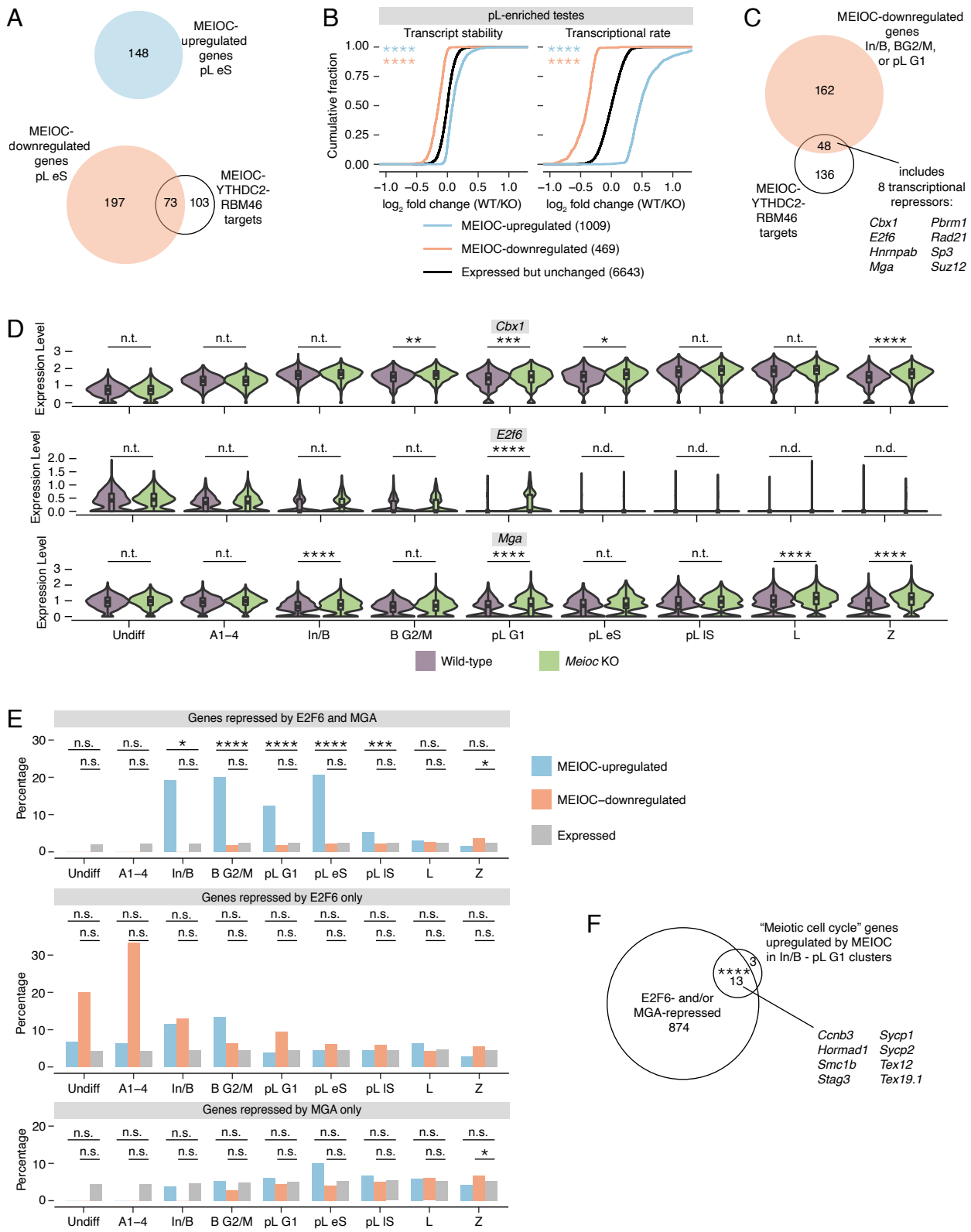
A
148
MEIOC-upregulated genes pL eS
MEIOC-downregulated genes pL eS
197
73
103
MEIOC-YTHDC2-RBM46 targets
B
pL-enriched testes
Transcript stability
Transcriptional rate
Cumulative fraction
log2 fold change (WT/KO)
MEIOC-upregulated (1009)
MEIOC-downregulated (469)
Expressed but unchanged (6643)
C
MEIOC-downregulated genes In/B, BG2/M, or pL G1
162
48
136
MEIOC-YTHDC2-RBM46 targets
includes 8 transcriptional repressors:
Cbx1 Pbrm1 E2f6 Rad21 Hnrnpab Sp3 Mga Suz12
D
Cbx1
E2f6
Mga
Expression Level
Undiff
A1–4
In/B
B G2/M
pL G1
pL eS
pL IS
L
Z
Wild-type
Meioc KO
E
Genes repressed by E2F6 and MGA
Genes repressed by E2F6 only
Genes repressed by MGA only
Percentage
MEIOC-upregulated
MEIOC–downregulated
Expressed
F
"Meiotic cell cycle" genes upregulated by MEIOC in In/B - pL G1 clusters
3
13
E2F6- and/or MGA-repressed 874
Ccnb3 Sycp1 Hormad1 Sycp2 Smc1b Tex12 Stag3 Tex19.1

1075 **Figure 3: MEIOC-YTHDC2-RBM46's repression of *E2f6* and *Mga* mRNA relieves E2F6-**
1076 **and MGA-mediated transcriptional repression.**
1077
1078 **A:** Venn diagram comparing MEIOC-upregulated and -downregulated genes in pL eS cluster to
1079 MEIOC-YTHDC2-RBM46 targets. The majority of genes whose transcript abundance changes
1080 in response to MEIOC are not directly targeted by MEIOC-YTHDC2-RBM46.
1081 **B:** Cumulative distribution of $\log_2$ fold change (WT/ *Meioc* KO) for transcript stability (left) and
1082 transcriptional rate (right) for MEIOC-upregulated and MEIOC-downregulated genes compared
1083 to genes that expressed but do not change in response to MEIOC. Transcript stabilities and
1084 transcriptional rates were estimated using bulk RNA-seq data from preleptotene-enriched testes.
1085 Asterisks represent comparison of color-matched gene set to expressed but not regulated gene
1086 set.
1087 **C:** Identification of MEIOC-YTHDC2-RBM46 targets that are downregulated by MEIOC in
1088 In/B, B G2/M, and/or pL G1 clusters. Of this set, 8 mRNAs encode proteins that have been
1089 reported to function as transcriptional repressors.
1090 **D:** Expression levels for PRC1.6 subunits *Cbx1*, *E2f6*, and *Mga* in wildtype vs. *Meioc*-null cells
1091 in all germ cell clusters identified. *Cbx1*, *E2f6*, and *Mga* are downregulated by MEIOC in the
1092 In/B, B G2/M, and/or pL G1 clusters (adj. $P < 0.05$).
1093 **E:** Percentage of genes repressed by E2F6 and MGA (top), E2F6 only (center), and MGA only
1094 (bottom) among MEIOC-upregulated, MEIOC-downregulated, and expressed genes. E2F6-
1095 repressed genes and MGA-repressed genes were identified via reanalysis of published ChIP-seq
1096 and RNA-seq datasets from mouse embryonic stem cells (Dahlet et al., 2021; Stielow et al.,
1097 2018; Qin et al., 2021).
1098 **F:** Overlap between E2F6- and/or MGA-repressed genes and the "meiotic cell cycle" genes
1099 upregulated by MEIOC in In/B, B G2/M, and pL G1 clusters. Example genes that fall within this
1100 overlap are listed.
1101
1102 *, adj. $P<0.05$; **, adj. $P<0.01$; ***, adj. $P<0.001$; ****, adj. $P<0.0001$; n.s., not significant; n.t.,
1103 not tested (comparison was excluded from statistical testing because $\log_2$ fold change> -0.1 and
1104 <0.1); n.d., not detected (transcript expressed in <25% cells in each population being compared).

Figure 4

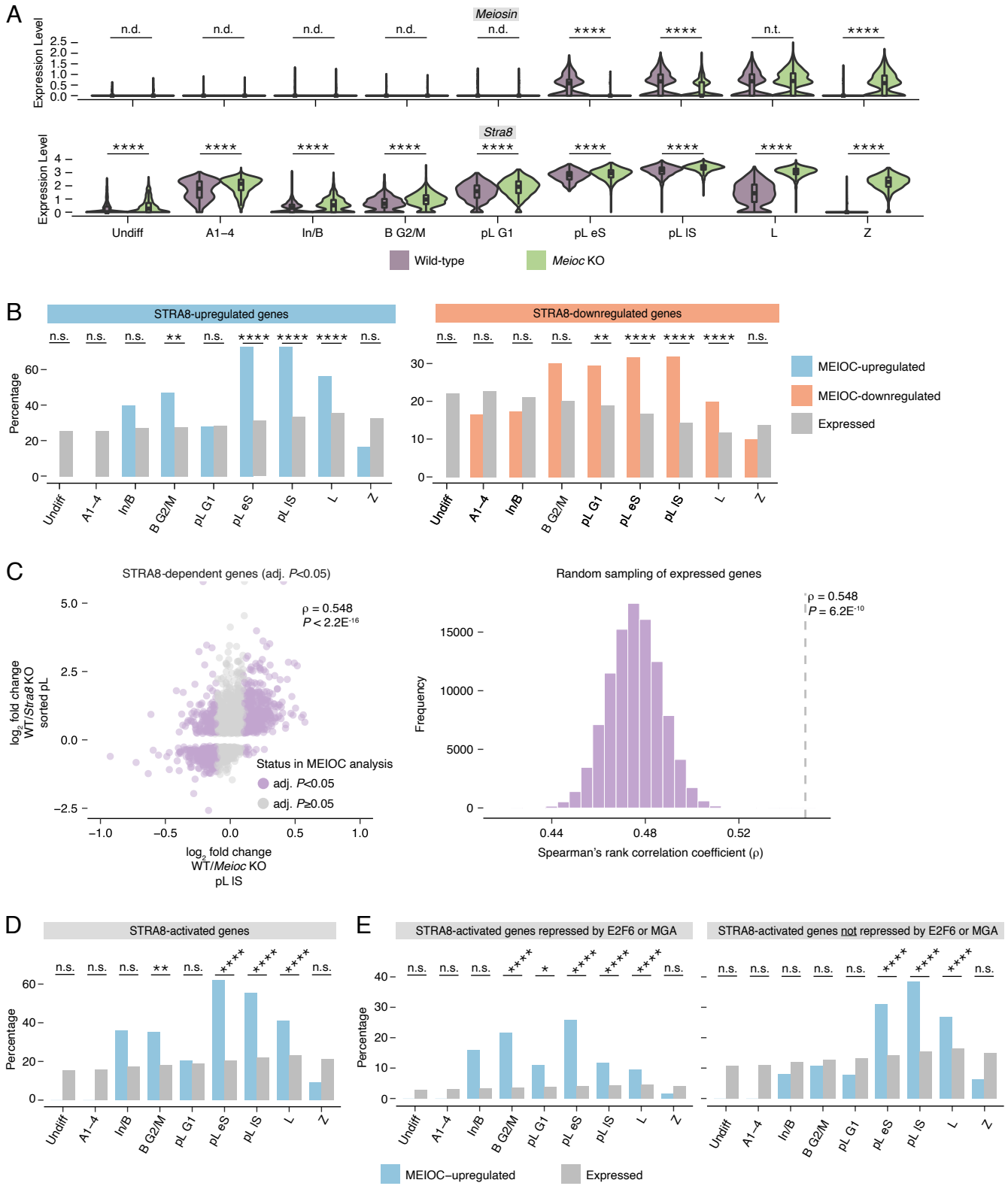
A
Meiosin
Stra8
Expression Level
n.d.
n.t.
****
Undiff
A1–4
In/B
B G2/M
pL G1
pL eS
pL lS
L
Z
Wild-type
Meioc KO
B
STRA8-upregulated genes
STRA8-downregulated genes
n.s.
**
Percentage
MEIOC-upregulated
MEIOC-downregulated
Expressed
C
STRA8-dependent genes (adj. P<0.05)
ρ = 0.548
P < 2.2E-16
log2 fold change WT/Stra8 KO sorted pL
log2 fold change WT/Meioc KO pL lS
Status in MEIOC analysis
adj. P<0.05
adj. P≥0.05
Random sampling of expressed genes
ρ = 0.548
P = 6.2E-10
Frequency
Spearman's rank correlation coefficient (ρ)
D
STRA8-activated genes
E
STRA8-activated genes repressed by E2F6 or MGA
STRA8-activated genes not repressed by E2F6 or MGA
MEIOC–upregulated
Expressed

1105 **Figure 4: MEIOC's derepression of *Meiosin* gene expression enhances activation of the**
1106 **STRA8-MEIOSIN transcriptional program.**
1107
1108 **A:** Expression levels of *Meiosin* and *Stra8* in wild-type and Meioc KO in all germ cell clusters.
1109 Clusters marked as "not done" (n.d.) did not meet expression thresholds set for statistical testing.
1110 **B:** Percentage of STRA8-upregulated and -downregulated genes in MEIOC-upregulated, -
1111 downregulated, and expressed genes from scRNA-seq analysis. STRA8-upregulated and -
1112 downregulated genes were identified via reanalysis of bulk RNA-seq data from wild-type and
1113 Stra8 KO sorted preleptotene spermatocytes from Kojima et al., 2019.
1114 **C:** Left panel, correlation between MEIOC scRNA-seq analysis of the pL lS cluster and STRA8
1115 bulk RNA-seq analysis of sorted preleptotene spermatocytes. Analysis was limited to genes that
1116 were statistically dependent on STRA8 (adj. $P<0.05$). P value represents the probability that
1117 Spearman rho does not equal 0. Right panel, distribution of correlations for gene sets obtained by
1118 random sampling of genes expressed in the scRNA-seq pL lS cluster and bulk RNA-seq sorted
1119 preleptotene spermatocytes. P value represents that probability of obtaining an equal or larger
1120 correlation by random sampling.
1121 **D:** Percentage of STRA8-activated genes in MEIOC-upregulated and expressed genes from
1122 scRNA-seq analysis. STRA8-activated genes were identified as those genes with STRA8-bound
1123 promoters (as identified by Kojima et al. (2019) via STRA8-FLAG ChIP-seq in preleptotene-
1124 enriched testes) and upregulated by STRA8 (as identified by reanalysis of bulk RNA-seq data
1125 from wild-type and Stra8 KO sorted preleptotene spermatocytes from Kojima et al., 2019).
1126 **E:** Percentage of STRA8-activated genes repressed by E2F6 or MGA (left), as well as STRA8-
1127 activated genes not repressed by E2F6 or MGA (right), in MEIOC-upregulated and expressed
1128 genes.
1129
1130 *, adj. $P<0.05$; **, adj. $P<0.01$; ***, adj. $P<0.001$; ****, adj. $P<0.0001$; n.s., not significant; n.t.,
1131 not tested (comparison was excluded from statistical testing because $\log_2$ fold change> -0.1 and
1132 <0.1); n.d., not detected (transcript expressed in <25% cells in each population being compared).
1133

Figure 5

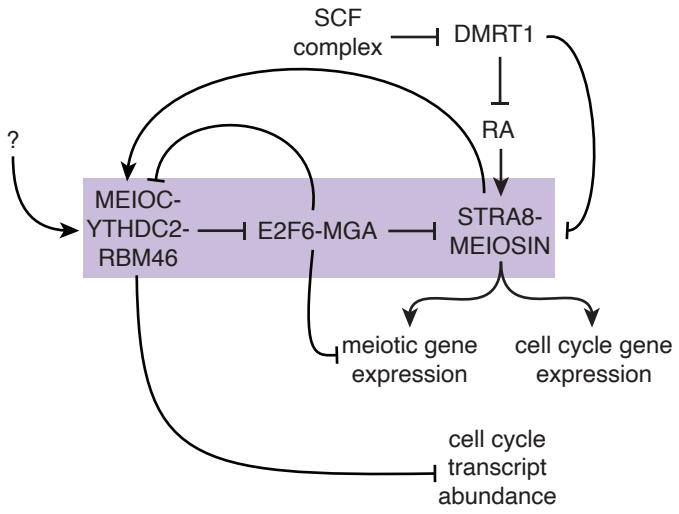
SCF
complex
DMRT1
RA
?
MEIOC-
YTHDC2-
RBM46
E2F6-MGA
STRA8-
MEIOSIN
meiotic gene
expression
cell cycle gene
expression
cell cycle
transcript
abundance

1134 **Figure 5: Model for MEIOC-YTHDC2-RBM46 enhancing spermatogenic cells'**
1135 **competence to transition from mitosis to meiosis in response to retinoic acid.**
1136
1137 MEIOC-YTHDC2-RBM46 destabilize *E2f6* and *Mga* mRNA and thereby inhibit E2F6 and
1138 MGA's repression of transcription at genes involved in meiosis, including *Meiosin* and *Meioc*. In
1139 parallel, the SCF complex degrades DMRT1 and consequently inhibits DMRT1's repression of
1140 retinoic acid (RA)-dependent transcription as well as *Stra8* and *Meiosin* gene expression.
1141 Retinoic acid activates *Stra8* and *Meiosi*n gene expression. This activates the STRA8-MEIOSIN
1142 transcription factor, which drives the transcription of cell cycle genes as well as meiotic genes,
1143 many of which were previously repressed by E2F6 and MGA. MEIOC's repression of cell cycle
1144 transcripts also contributes to the establishment of a meiosis-specific cell cycle program in
1145 meiotic prophase I. The question mark denotes undefined molecular regulation that activates
1146 MEIOC-YTHDC2-RBM46 before retinoic acid activates STRA8-MEIOSIN transcriptional
1147 activity and the transition from mitosis to meiosis. Purple box highlights the novel regulation
1148 identified in this study that facilitates competence for the mitosis-to-meiosis transition.